Ser[12]-Pro motif in this protein. This enhances the stability and hence the transcriptional activity of Oct4. Our present data thus suggest that Pin1 is indeed a putative regulator of the self-renewal and proliferation of pluripotent stem cells.

EXPERIMENTAL PROCEDURES

Colony Formation Analysis—Human iPS cells were obtained from the RIKEN BioResource Center (clone no. 201B7) (19). Cells were cultured in human embryonic stem cell culture medium (KnockOut Dulbecco's modified Eagle's medium (Invitrogen)) supplemented with 20% KnockOut SR (Invitrogen), 1% GlutaMAX (Invitrogen), 100 μM nonessential amino acids (Invitrogen), 50 μM β-mercaptoethanol, and 10 ng/ml basic fibroblast growth factor). Murine ES cells were cultured in human embryonic stem cell culture medium (KnockOut Dulbecco's modified Eagle's medium supplemented with 15% KnockOut SR, 1% GlutaMAX (Invitrogen), 100 μM nonessential amino acids, 50 μM β-mercaptoethanol, and 1000 units/ml recombinant human leukemia inhibitory factor) (20). Colony formation was scored by counting the number of alkaline phosphatase (AP)-positive colonies as described previously (21). The number of cells per colony was determined by manually counting the number of DAPI-stained cells (21).

Cell Reprogramming—MRC5 fibroblasts were transduced with retroviral vectors encoding reprogramming factors as described previously (19). Briefly, the retroviral vector plasmids pMXs-hOct4, pMXs-hSOX2, pMXs-hKLF4, pMXs-hcMYC (Addgene), and pVSV-G were introduced into Plat-E cells using Effectene transfection reagent (Qiagen). After 48 h, virus-containing supernatants were passed through a 0.45-μm filter and supplemented with 10 μg/ml hexadimethrine bromide (polybrene). Cells were seeded at 6×10^5 cells per 60 mm dish at 24 h before incubation in the virus/polybrene-containing supernatants for 16 h. After 6 days, cells were plated on irradiated mouse embryonic fibroblasts, and culture medium was replaced with the hESC culture medium 24 h later. Cells were maintained at 37 °C and 5% CO_2 for 30 days.

Construction of Expression Vectors—Oct4 cDNA was subcloned into pcDNA3-HA expression vector (Invitrogen). Expression constructs of Oct4 were as follows: pcDNA-HA-Oct4 wild-type, amino acids 1–360; pcDNA-HA-Oct4 ΔC, amino acids 1–297; pcDNA-HA-Oct4 ΔN1, amino acids 138–360; pcDNA-HA-Oct4 ΔN2, amino acids 113–360; and pcDNA-HA-Oct4 ΔN3, amino acids 34–360. pcDNA-HA-Oct4-S12A was generated by KOD-Plus Mutagenesis Kit (Toyobo, Osaka, Japan) according to the manufacturer's instructions. The primers were 5′-CGCCCCCTCCAGGTGGT-3′ (forward) and 5′-CGAAGGCAAAATCTGAAGCC-3′ (reverse).

Gene Reporter Assay—A pGL3-fgf4 reporter plasmid containing an Oct-SOX binding cassette and the firefly luciferase gene was transfected with pRL-CMV (22). The −2601/+1 (nucleotide positions indicated with respect to the +1 translation start site) genomic fragment of the Oct4 promoter upstream region was amplified by PCR from human lymphocyte genomic DNA and cloned into the KpnI/HindIII sites of the pGL4-basic reporter plasmid (Promega, Madison, WI) as described previously (23). The primer sets were as follows: 5′-CCTGGTACCAGGATGGCAAGCTGAGAAACACTG-3′ and 5′-TCGCAAGCTTGCGAAGGGACTACTCAAC-3′. Cells were transfected with reporter plasmid vectors using Effectene (Qiagen) or Xfect Stem (Clontech). One day after transfection, the cells were resuspended in passive lysis buffer (Promega) and incubated for 15 min at room temperature. Luciferase activities were measured with a Dual-Luciferase reporter assay system (Promega) in accordance with the manufacturer's instructions.

GST Pulldown Assay and Immunoprecipitation Analysis—Cells were lysed with GST pulldown buffer (50 mM HEPES (pH 7.4), 150 mM NaCl, 10% glycerol, 1% Triton X-100, 1.5 mM $MgCl_2$, 1 mM EGTA, 100 mM NaF, 1 mM Na_3VO_4, 1 mM DTT, 5 μg/ml leupeptin, 1 μg/ml pepstatin, and 0.2 mM PMSF) and incubated with 30 μl of glutathione-agarose beads containing either GST-Pin1 or GST at 4 °C for 2 h. The precipitated proteins were then washed three times with lysis buffer and subjected to SDS-PAGE. For immunoprecipitation, cells were lysed with Nonidet P-40 lysis buffer (10 mM Tris HCl (pH 7.4), 100 mM NaCl, 0.5% Nonidet P-40, 1 mM Na_3VO_4, 100 mM NaF, 5 μg/ml leupeptin, 1 μg/ml pepstatin, and 0.2 mM PMSF). Cell lysates were incubated for 1 h with protein A/G-Sepharose·nonimmunized IgG complexes. Supernatant fractions were recovered and immunoprecipitated with 5 μg of anti-Myc antibody and 30 μl protein A/G-Sepharose. After washing three times with lysis buffer, the pellets were analyzed by SDS-PAGE.

Proteomics Analysis—Human iPS cell lysates were processed for immunoprecipitation with a monoclonal anti-Pin1 antibody (clone 257417, R&D Systems) at 4 °C for 3 h followed by SDS-PAGE. Gel lanes corresponding to the region from ~30 to 150 kDa were systematically excised, and the pieces were reduced, alkylated, and trypsinized. Peptides were analyzed by the linear ion trap Orbitrap hybrid mass spectrometer (Thermo Scientific). Protein identification was performed by peptide

FIGURE 1. **Pin1 is preferentially expressed in human iPS cells.** *A*, immunoblotting analysis of Oct4, SOX2, and Pin1 in MRC5 and MRC5-derived iPS cells. Actin was used as a loading control. *iPSC*, induced pluripotent stem cells; *EV*, empty vector. *B*, immunofluorescent analysis of Pin1 and SOX2 in human iPS cells. Representative images of phase-contrast microscopy and fluorescent immunocytochemistry for SOX2 (*red*) and Pin1 (*green*) are shown. Nuclei are indicated by DAPI staining (*blue*). Note that Pin1 is highly expressed in SOX2-positive pluripotent stem cells. *C* and *D*, Pin1 expression enhances 4F (Oct4, SOX2, Klf4, and c-Myc)-induced iPS cell induction. MRC5 fibroblasts were infected with retrovirus vectors encoding 4F and co-infected with those encoding either empty vector or Pin1. A representative picture of colony formations stained with AP is shown (*C*). The numbers of AP-positive colonies were scored in three independent experiments (*D*). Note that the co-introduction of Pin1 with 4F increases the frequency of iPS colony formation. *E* and *F*, MRC5 fibroblasts were infected with retrovirus vectors encoding 4F and co-infected with those encoding empty vector, HA-tagged wild-type Pin1, or its W34A or K63A mutants. The expression levels of HA-Pin1 or its mutants in infected MRC5 cells were analyzed by immunoblotting analysis with anti-HA antibody (*E*). The number of AP-positive colonies was scored in three independent experiments (*F*). *G*, teratoma tissue derived from human iPS cells induced by 4F and Pin1. iPS cells were transplanted subcutaneously into immunodeficient mice (2×10^6/mouse). Representative images of hematoxylin and eosin stained tumor with light microscope (200×) are shown.

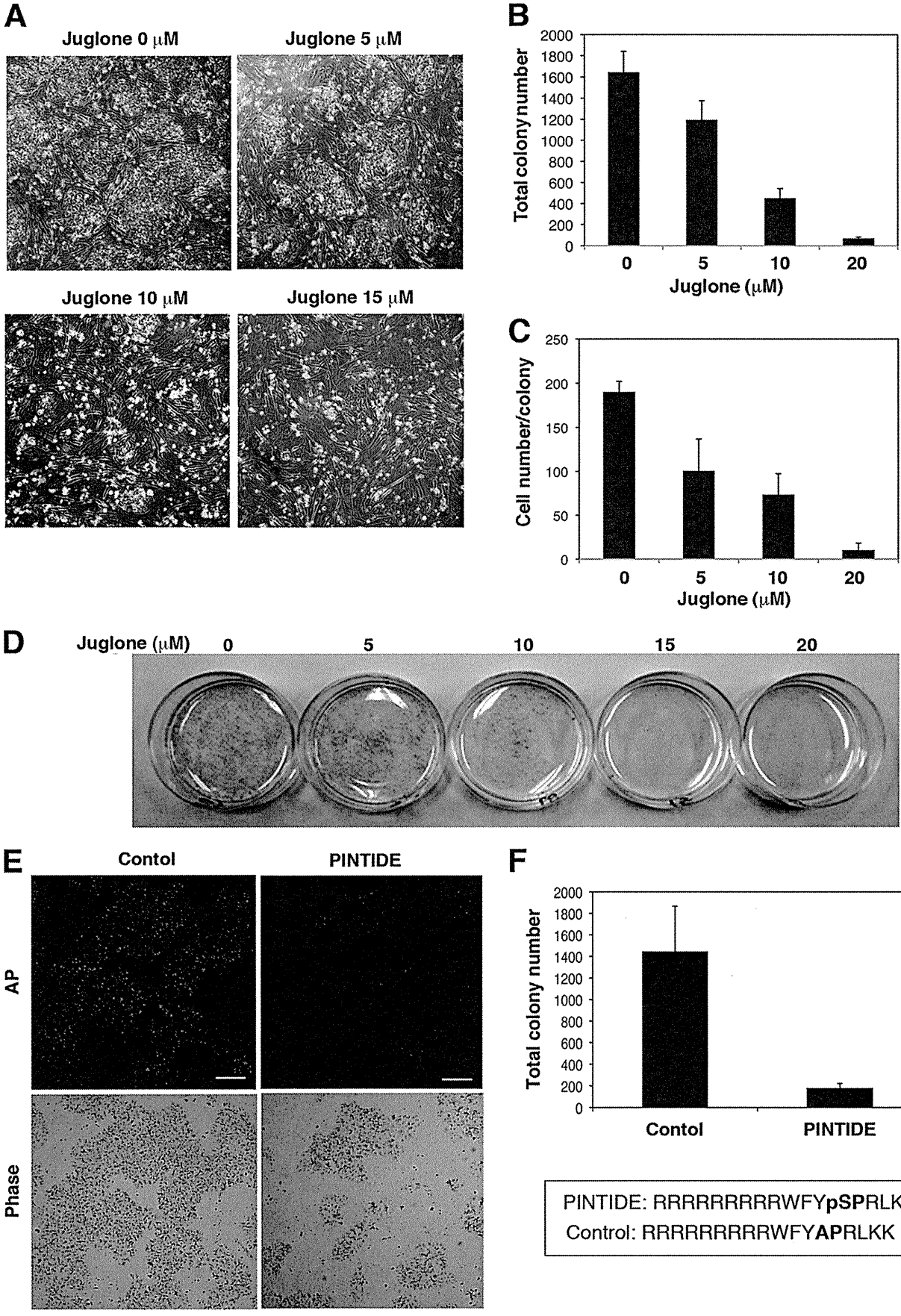

mass fingerprinting with the Mascot and Aldente search algorithms.

Quantitative Real-time PCR—Total RNA was extracted with TRIzol reagent (Invitrogen) according to the manufacturer's protocol. cDNA was synthesized using a cDNA synthesis kit (Toyobo, Osaka, Japan) and subjected to RT-PCR analysis with the SYBR Premix Ex gent Kit TaqII (Takara Bio, Shiga, Japan) using an Applied Biosystems 7300 real-time PCR System. The primer sets used were as follows: mOct4, 5′-CGTGTGAGGTGGAGTCTGGAGACC-3′ and 5′-ACTCGAACCACATCCTTCTCTAGCC-3′; mGAPDH, 5′-CCATGGAGAAGGCTGGGG-3′ and 5′-CAAAGTTGTCATGGATGACC-3′.

Teratoma Formation—Cells were harvested using accutase, collected into tubes, and centrifuged. The pellets were then suspended in human ESC culture medium. Fox Chase severe combined immunodeficiency mice (CREA, Tokyo, Japan) were injected with 2×10^6 cells mixed with an equal volume of Matrigel (BD Biosciences). Frozen tumor tissues embedded in optimum cutting temperature compound were sliced by cryosectioning and stained with hematoxylin and eosin.

RESULTS

Pin1 Is Induced upon Cellular Reprogramming and Enhances Generation of iPS Cells—To examine the role of Pin1 in cellular reprogramming and pluripotency, we initially investigated the expression levels of this prolyl isomerase in human iPS cells. Pin1 was found to be significantly induced upon the generation of iPS cells derived from MRC5 human fibroblasts (Fig. 1*A*). Immunofluorescent analysis further revealed that Pin1 is selectively expressed in SOX2-positive pluripotent stem cells, whereas its expression was found to be significantly suppressed in the surrounding SOX2-negative differentiated cells (Fig. 1*B*). These results indicate that Pin1 is preferentially expressed in reprogramming stem cells.

We next evaluated whether Pin1 affects the reprogramming of somatic cells into iPS cells. The co-infection of a Pin1-encoding retrovirus vector with those encoding four defined reprogramming factors (4F; SOX2, Oct4, Klf-4, and c-Myc) (24) notably boosted the generation of AP-positive iPS cell colonies compared with an induction of human fibroblast MRC5 cells with only four iPS factors (Fig. 1, *C* and *D*). We next performed a parallel experiment using either a WW-domain (binding domain) mutant (W34A) or a peptidyl prolyl isomerase-domain (catalytic domain) mutant (K63A) of Pin1. We confirmed the equivalent expression of each of these mutants and wild-type Pin1 (Fig. 1*E*). Neither of these mutants could boost iPS cell colony formation to the level seen with wild-type Pin1 (Fig. 1*F*), indicating that both the WW and PPIase domains are required for this function.

To test pluripotency *in vivo*, we transplanted 4F plus Pin1-introduced iPS cells subcutaneously into the dorsal flanks of immunodeficient mice. Nine weeks after injection, we observed teratoma formation composed of various tissues including gut-like epithelial tissues (endoderm), striated muscle (mesoderm), cartilage (mesoderm), neural tissues (ectoderm), and epidermal tissues (ectoderm) (Fig. 1*G*). These results indicate that the expression of Pin1 with defined reprogramming factors accelerates the frequency of iPS cell generation.

Pin1 Is Required for Pluripotent Stem Cell Self-renewal and Colony Formation—We next addressed whether Pin1 indeed plays any roles in the self-renewal of human iPS cells. iPS cells were dissociated with accutase and then plated at a clonal density in the presence of several concentrations of the selective Pin1 inhibitor juglone (5-hydroxy-1,4-naphthoquinone) (25, 26). The blockade of Pin1 by juglone considerably reduced both the numbers and size of the colonies in a dose-dependent manner (Fig. 2, *A–C*). It was notable also that the concentration of juglone used did not illicit nonspecific toxic effects in the feeder mouse embryonic fibroblast cells (Fig. 2*A* and data not shown). The effect of Pin1 inhibition upon colony formation was also confirmed in feeder-free cultures of human iPS cells by AP staining (Fig. 2*D*). Moreover, treatment with the Pin1 inhibitory phosphopeptide PINTIDE (27), but not a nonphosphorylated control peptide, significantly reduced the colony formation of human iPS cells (Fig. 2, *E* and *F*).

We next investigated the effects of Pin1 inhibition upon colony formation in murine ES cells. The blockade of Pin1 by juglone significantly reduced the colony numbers in two different murine ES cell types, BDF2 and R1 (Fig. 3*A*). The adenovirus-mediated transduction of a GFP-fused dominant-negative Pin1 (GFP-dnPin1) (28), but not a GFP control, significantly suppressed colony formation in murine ES (R1) cells manifesting as a considerable reduction in both the numbers and colony size of the murine ES cells (Fig. 3, *B–D*). These results together demonstrate that Pin1 is indispensable for the self-renewal and proliferation of pluripotent stem cells.

Pin1 Functions in Maintenance of Pluripotency—We next asked whether Pin1 has any roles in the maintenance of pluripotency in stem cells. Human iPS cells were dissociated and then cultured for 5 days to form colonies. When human iPS cells are cultured in hES medium supplemented with basic fibroblast growth factor, the overwhelming majority of the cells in the colonies are undifferentiated (Fig. 4*A*). However, treatment with juglone resulted in aberrant cell differentiation resulting in a "mosaic pattern" of iPS cell colonies following AP staining (Fig. 4*A*). Similarly, the adenovirus-mediated transduction of GFP-dnPin1, but not a GFP control, prominently reduced the number of AP-positive undifferentiated cells in murine ES cell colonies (Fig. 4*B*). These results together indicate that Pin1 can sustain pluripotent stem cells in an undifferentiated state in addition to the enhancement of self-renewal.

FIGURE 2. **Defective self-renewal of human iPS cells caused by Pin1 inhibition.** *A–C*, human iPS cells were dissociated with accutase and then plated on a feeder cell layer at a clonal density in the presence of the indicated concentrations of juglone for 3 days. Colony formation was analyzed by phase-contrast microscopy (*A*). The number of colonies was counted at 3 days after treatment (*B*). The number of cells per colony was determined by manually counting the DAPI-stained cells (*C*). Data are the mean ± S.E. *D*, human iPS cells were plated at a clonal density on the feeder-free culture in the presence of the indicated concentrations of juglone followed by AP staining. *E* and *F*, human iPS cells were dissociated with accutase and then plated on feeder-free dishes at a clonal density in the presence of 50 μg/ml of the Pin1 inhibitory phosphopeptide PINTIDE (RRRRRRRRRWFYpSPRLKK) or a nonphosphorylated control peptide (RRRRRRRRRWFYAPRLKK) for 48 h (*E*). AP-positive colony numbers were scored (*F*). Data are the mean ± S.E. *Scale bar*, 50 μm.

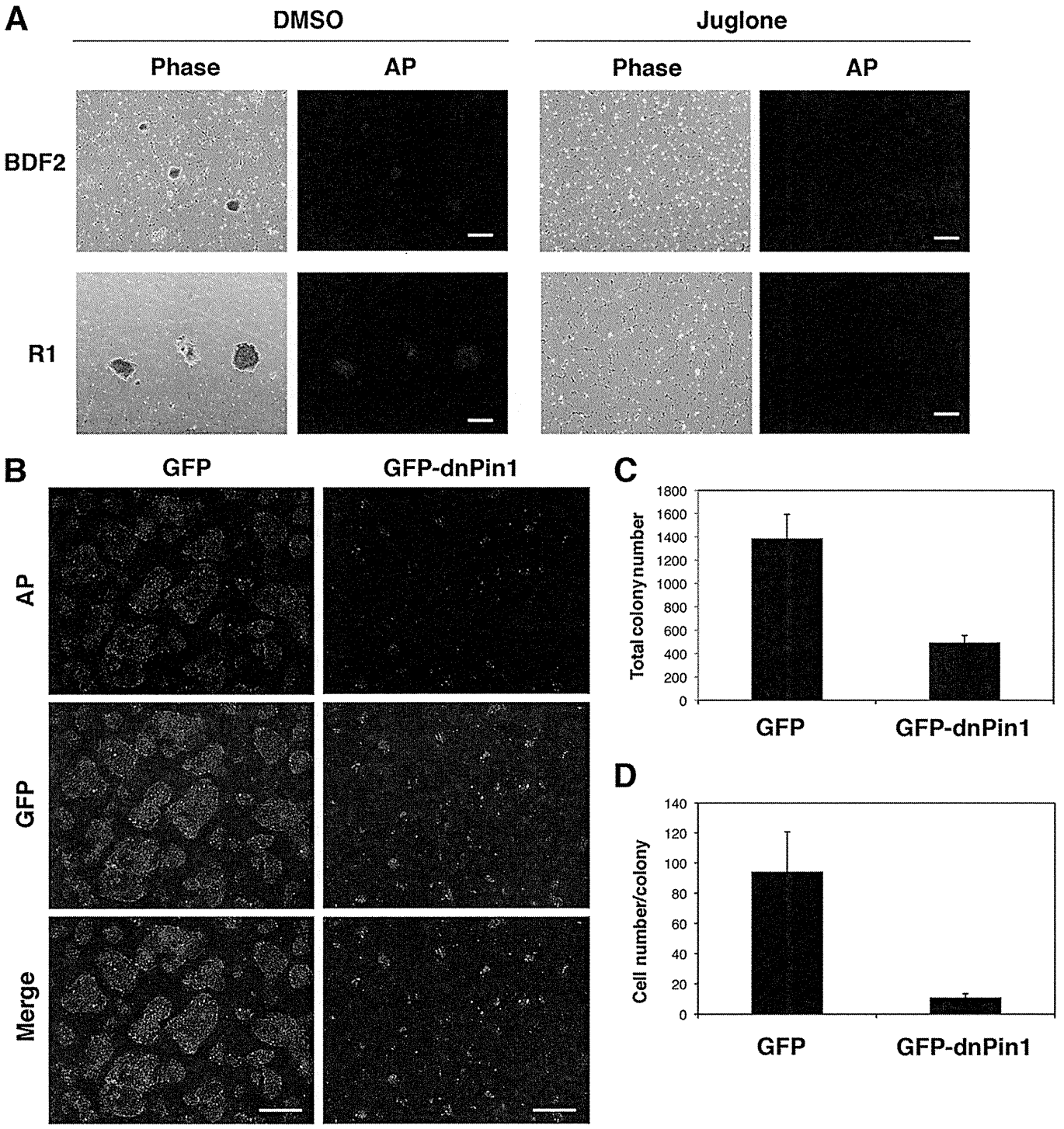

FIGURE 3. **Pin1 inhibition suppresses colony formation in murine ES cells.** *A*, two different murine ES cell types (BDF2 and R1) were plated on gelatin-coated dishes and treated with either DMSO or juglone (10 μM). Colonies were stained with AP (*red*). *Scale bar*, 200 μm. *B–D*, murine ES cells (R1) were infected with an adenovirus vector encoding either GFP or GFP-dnPin1 (3000 viral particles/cell). The cells were then stained with AP (*red*) and DAPI and analyzed by immunofluorescent microscopy (*B*). *Scale bar*, 200 μm. The total colony number (*C*) and the number of cells per colony (*D*) were then determined. Data are the mean ± S.E.

Identification of Pin1 Binding Proteins in Human iPS Cells—Our initial data indicated that Pin1 could enhance the function of reprogramming factors during the induction and maintenance of pluripotency. We next identified the substrates targeted by Pin1 in human iPS cells. Using a monoclonal Pin1 antibody, we co-immunoprecipitated proteins from human iPS cell lysates treated with a phosphatase inhibitor mixture. These isolated immune complexes were then boiled and resolved by one-dimensional SDS-PAGE, and the proteins were visualized using silver staining. Continuous regions of the gel corresponding to proteins of ~30 to 150 kDa in size were systematically excised (Fig. 5*A*), digested with trypsin, and analyzed in a linear

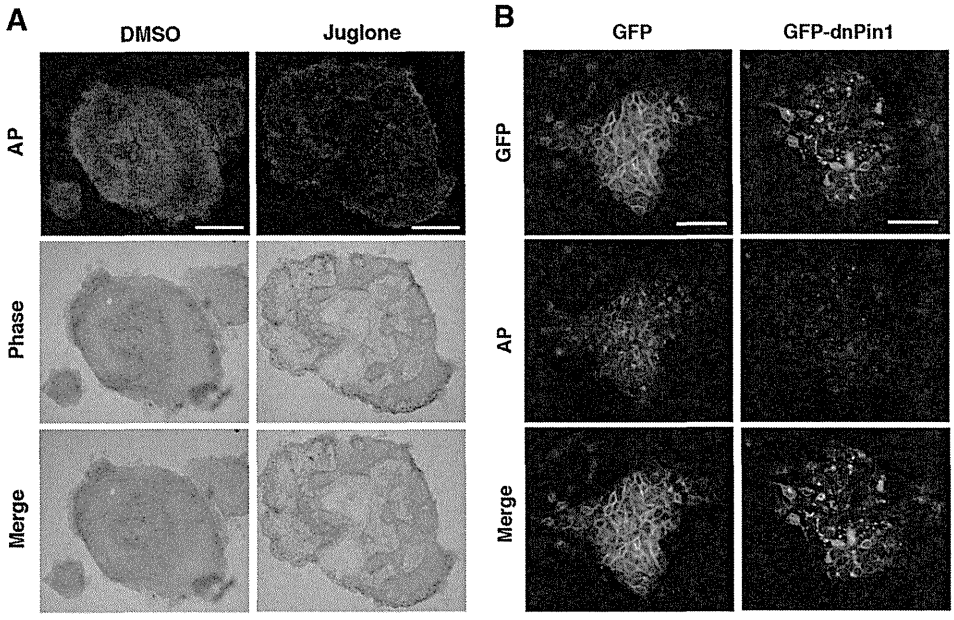

FIGURE 4. **Pin1 inhibition leads to the aberrant cell differentiation of human iPS cells.** *A*, human iPS cells were cultured for 5 days before forming colonies and then treated with either DMSO or juglone (10 μM) for 3 days. The cells were then stained with AP (*red*). Representative images of phase-contrast microscopy and fluorescent immunocytochemistry are shown. *Scale bar*, 200 μm. *B*, mouse ES cells were cultured for 2 days before forming colonies and then infected with an adenovirus vector encoding either GFP or GFP-dnPin1 (3000 viral particles/cell). After 48 h, the cells were then stained with AP (*red*) and DAPI (*blue*) and analyzed by immunofluorescent microscopy. *Scale bar*, 50 μm.

ion trap (LTQ) Orbitrap hybrid mass spectrometer. Peptide mass fingerprinting with the Mascot and Aldente search algorithms subsequently identified 23 Pin1 interacting proteins in human iPS cells (Fig. 5*B*). Notably, these Pin1-binding proteins included the pluripotent transcription factor Oct4. Because Oct4 has been shown to be a master regulator of pluripotency (29), we decided to further analyze the Oct4-Pin1 interaction.

Pin1 Binds and Regulates Protein Stability of Oct4—To further characterize the Oct4-Pin1 interaction, a GST pulldown analysis was initially performed. We found that recombinant GST-Pin1, but not GST alone, binds Oct4. This association was completely abolished by pretreatment of the cell lysates with calf intestine alkaline phosphatase (Fig. 6*A*), indicating that Pin1 binds phosphorylated Oct4. Immunofluorescence analysis further demonstrated that Pin1 co-localizes with Oct4 in the nuclei of iPS cells (Fig. 6*B*). Pin1 has been shown to regulate the stability of its substrate proteins upon binding (17), and we thus addressed whether this was the case for Oct4. Cycloheximide analysis using HeLa cells transfected with Oct4 alone or co-transfected with Oct4 and Pin1 revealed that the protein half-life of Oct4 is significantly enhanced in cells co-expressing Pin1 (Fig. 6*C*). Moreover, immunoprecipitation analysis with cells co-transfected with Oct4 and Myc-tagged ubiquitin, with or without Pin1 co-transfection, further revealed that Pin1 overexpression significantly reduces the polyubiquitination of the Oct4 protein (Fig. 6*D*). Consistently, the Oct4 protein expression level was significantly reduced in human iPS cells treated with juglone as compared with control cells (Fig. 6*E*). These results together confirm that Pin1 enhances the protein stability of Oct4 by suppressing ubiquitin proteasome-mediated proteolysis.

We next investigated the gene expression profile of Oct4 during the inhibition of Pin1. Murine ES cells were transfected with pGL4-Oct4-2601 promoter (harboring a genomic fragment of the Oct4 gene 5′-upstream region) and treated or not with juglone. Pin1 inhibition by juglone did not affect the transcriptional activity of the Oct4 promoter (Fig. 6*F*). Consistently, the results of parallel quantitative RT-PCR analysis demonstrated that the Oct4 mRNA level was not significantly altered by Pin1 inhibition (Fig. 6*G*), whereas the Oct4 protein level was significantly reduced by juglone treatment, as revealed by immunoblot analysis (Fig. 6*H*). These results together indicate that Pin1 regulates the protein stability of Oct4 but not Oct4 transcription.

We next addressed whether Pin1 enhances the transcriptional activity of the Oct4 protein. A luciferase reporter assay using the Oct-Sox enhancer region derived from the FGF4 gene was performed in HeLa cells co-transfected with Oct4, SOX2 or Pin1. Although the sole expression of Pin1 had no significant effects, the co-expression of Oct4 and Pin1 produced a significant increase in reporter activity in a dose-dependent fashion (Fig. 6*I*). This indicated that Pin1 promotes Oct4-mediated transcriptional activation. We performed a parallel experiment using the W34A and K63A Pin1 mutants. Neither of these mutants up-regulated the transcriptional activity of Oct4 to the levels seen with wild-type Pin1 (Fig. 6*J*), indicating that both the WW and PPIase domains are required for this function.

Pin1 Interacts with Ser^{12}-Pro motif of Oct4—To identify the specific Pin1 binding site within the Oct4 protein, we generated several Oct4 deletion mutants and performed GST-pulldown analysis. These experiments revealed that a C-terminal Oct4 deletion mutant (representing amino acids 1–297) could still bind Pin1, but that three extended N-terminal deletion mutants (amino acids 138–360, 113–360, or 34–360) failed to do so (Fig. 7*A*). These data indicate that Pin1 binds to Oct4 in the region between amino acids 1 and 34. Previous reports have indicated

A

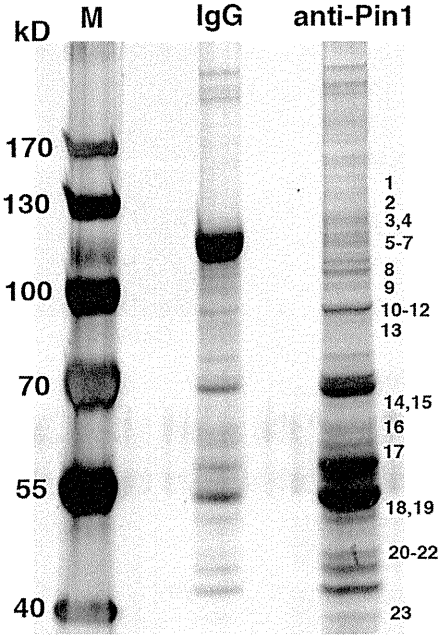

B

No.	Accession No.	Gene description	Predicted size
1	ADCY5_HUMAN	Adenylate cyclase type 5	138818
2	CCD40_HUMAN	Coiled-coil domain-containing protein 40	130033
3	PK3CA_HUMAN	Phosphatidylinositol-4,5-bisphosphate 3-kinase catalytic subunit alpha	124203
4	ZEB1_HUMAN	Zinc finger E-box-binding homeobox 1	123997
5	VINC_HUMAN	Vinculin	123722
6	RADIL_HUMAN	Ras-associating and dilute domain-containing protein	117351
7	UBP2L_HUMAN	Ubiquitin-associated protein 2-like	114465
8	DSG1_HUMAN	Desmoglein-1	113644
9	ENPP3_HUMAN	Ectonucleotide pyrophosphatase/phosphodiesterase family member 3	100059
10	ZN337_HUMAN	Zinc finger protein 337	86819
11	NASP_HUMAN	Nuclear autoantigenic sperm protein	85186
12	ZY11B_HUMAN	Protein zyg-11 homolog B	83921
13	MPEG1_HUMAN	Macrophage-expressed gene 1 protein	78587
14	FA13C_HUMAN	Protein FAM13C	65687
15	VPS45_HUMAN	Vacuolar protein sorting-associated protein 45	65036
16	ANR53_HUMAN	Ankyrin repeat domain-containing protein 53	59493
17	RPA34_HUMAN	DNA-directed RNA polymerase I subunit RPA34	54951
18	VIME_HUMAN	Vimentin	53619
19	KCAB1_HUMAN	Voltage-gated potassium channel subunit beta-1	46534
20	PRS8_HUMAN	26S protease regulatory subunit 8	45597
21	FKBP8_HUMAN	Peptidyl-prolyl cis-trans isomerase FKBP8	44534
22	PO5F1_HUMAN	POU domain, class 5, transcription factor 1 (OCT4)	38571
23	THAP1_HUMAN	THAP domain-containing protein 1	24928

FIGURE 5. **Identification of Pin1-binding proteins in human iPS cells.** *A* and *B*, lysates of human iPS cells were subjected to immunoprecipitation with either non-immunized control mouse IgG (IgG) or mouse anti-Pin1 monoclonal antibodies. Proteins bound to protein A/G-agarose beads were isolated, resolved by SDS-PAGE, and detected by silver staining (*A*). *M* indicates protein marker. Excised gel bands were digested with trypsin and analyzed on a linear ion trap (LTQ) Orbitrap hybrid mass spectrometer followed by peptide mass fingerprinting with the Mascot and Aldente search algorithms (*B*).

that Pin1 can bind only phosphorylated Ser/Thr-Pro motifs (17, 27) of which only one (Ser^{12}-Pro) exists between residues 1 and 34 in the Oct4 protein. Interestingly, this motif is conserved between various species including human, mouse, rat, and rabbit (Fig. 7*B*). We generated an Oct4 site-directed mutant at this site by substituting serine 12 for alanine (S12A). GST pulldown analysis subsequently revealed that Pin1 binds wild-type Oct4, but not its S12A mutant (Fig. 7*C*). These results confirm that Pin1 indeed bind the phosphorylated Ser^{12}-Pro motif of Oct4.

To further examine the functional interactions between Pin1 and Oct4 on this site, we next investigated the nature of the S12A mutant in terms of its protein expression in the presence of Pin1. HeLa cells were transfected with either wild-type Oct4 or its S12A mutant and co-transfected with Pin1. This was followed by immunoblotting analysis. We found that Pin1 increased the expression levels of wild-type Oct4, but not the S12A mutant (Fig. 7*D*).

DISCUSSION

In our present study, we report that Pin1 is an essential regulator of the self-renewal and maintenance of pluripotent stem cells. We further found the following: 1) Pin1 is induced upon the induction of human iPS cells; 2) the co-expression of Pin1 with defined reprogramming factors significantly enhances the

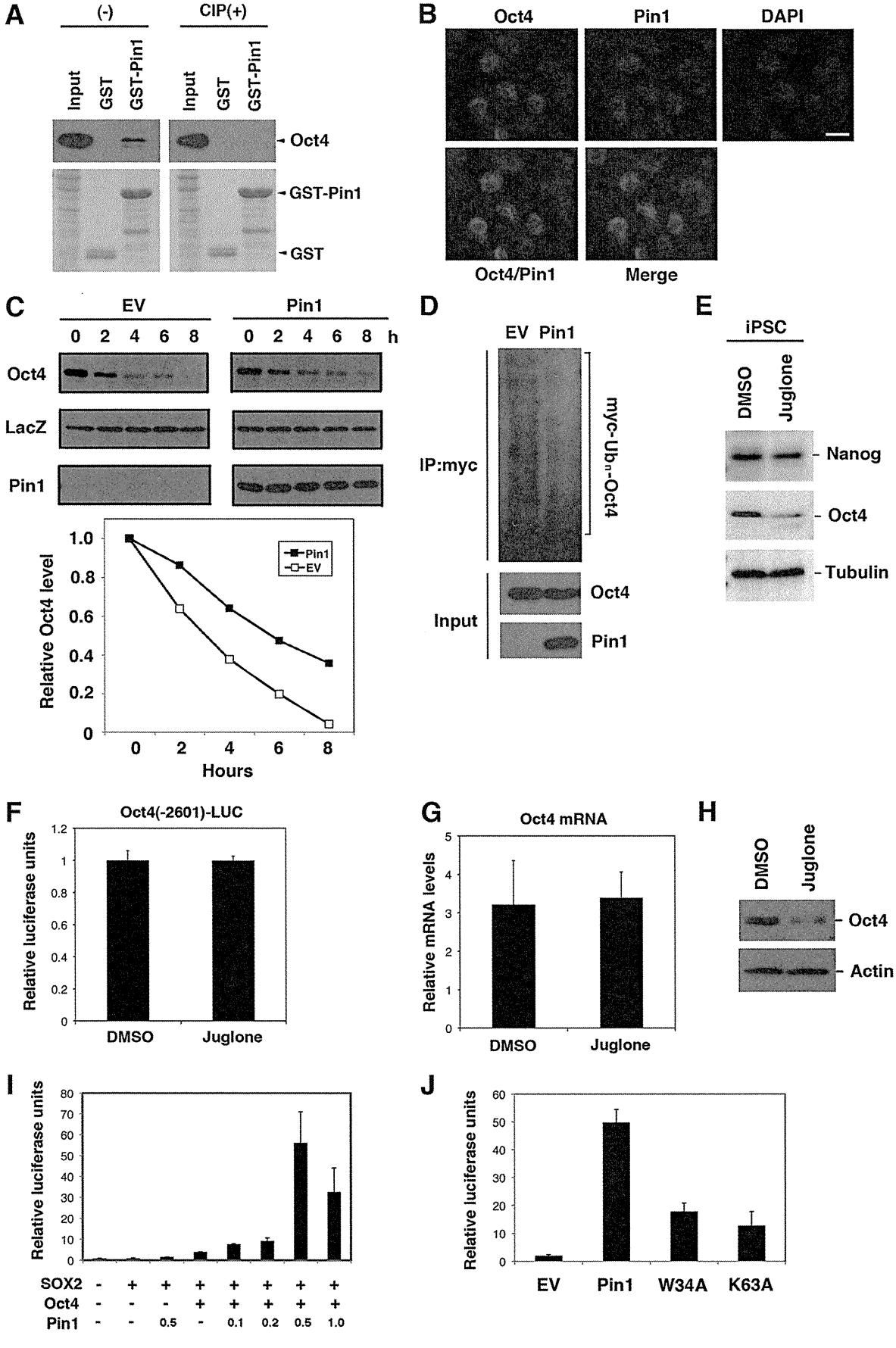

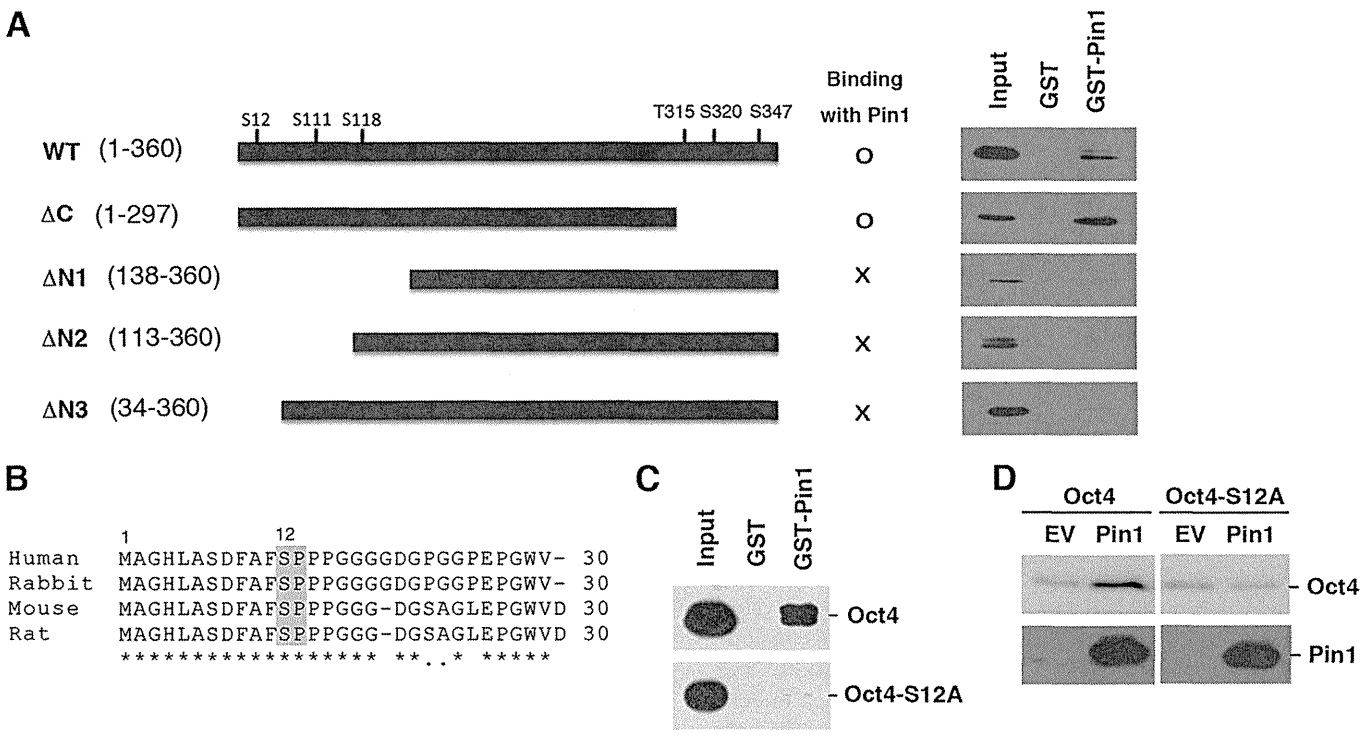

FIGURE 7. **Pin1 interacts with the Ser[12]-Pro motif of Oct4.** *A*, schematic representation of the Oct4 deletion mutants generated in this study (*left panel*). HeLa cells were transfected with the indicated Oct4 deletion mutants for 24 h. Cell lysates were then prepared and subjected to GST pulldown analysis with either GST or GST-Pin1 followed by immunoblotting analysis with Oct4 antibodies (*right panel*). *B*, amino acid sequence alignment of the human, rabbit, mouse, and rat Oct4 proteins. The conserved Ser[12]-Pro motifs are *boxed*. *C*, HeLa cells were transfected with the Oct4 site-directed mutant Oct4-S12A and subjected to GST pulldown analysis. *D*, HeLa cells were transfected with wild-type Oct4 or its S12A mutant with or without Pin1. After 24 h, the cells were subjected to immunoblotting analysis with an anti-Oct4 antibody.

frequency of iPS cell induction; 3) the blockade of Pin1 significantly inhibits the colony formation of dissociated human iPS cells and murine ES cells; 4) Pin1 inhibition leads to the aberrant cell differentiation in human iPS cells and murine ES cells after forming colonies; 5) Oct4 is a putative Pin1 substrate in human iPS cells; and 6) Pin1 interacts with Oct4 at its Ser[12]-Pro motif and facilitates its stability and enhanced transcriptional activity. Our findings thus uncover a novel role of Pin1 as a putative regulator of the self-renewal and survival of pluripotent stem cells via Oct4 function.

Our current results add to previous findings indicating that Pin1 is a multifunctional protein that mediates various phosphorylated proteins involved in divergent cellular processes (17). This implicates Pin1 as a modulator of multiple signaling pathways depending on the cell type and biological context. Indeed, we demonstrate in our present study that Pin1 is a crucial regulator of the phosphorylation-dependent intracellular signaling network that controls cellular stemness and pluripotency. Moreover, iPS cells induced by the expression of four Yamanaka factors (Oct4, SOX2, Klf4, and c-Myc) led to a high expression level of Pin1, and these cells were found to be dependent on Pin1 function. This suggests that Pin1 could be one of the crucial factors in the induction of iPS cells from somatic cells that functions by cooperating with reprogramming transcription factors.

FIGURE 6. **Pin1 interacts with phosphorylated Oct4 and enhances its transcriptional activity.** *A*, human iPS cell lysates treated or untreated with calf intestine alkaline phosphatase were subjected to GST pulldown analysis with either GST or GST-Pin1, followed by immunoblotting analysis with anti-Oct4 antibody (*upper panel*). Coomassie staining for the GST or GST-Pin1 used in the assay is shown in the *lower panel*. *B*, human iPS cells were fixed with 4% paraformaldehyde and then co-immunostained with monoclonal antibodies against Oct4 (*green*) and polyclonal antibodies against Pin1 (*red*). Cells were then analyzed by confocal microscopy. *Scale bar*, 10 μm. *C*, HeLa cells transfected with the indicated vectors and HA-LacZ cells were treated with cycloheximide and harvested at the indicated time points. This was followed by immunoblotting analysis with Oct4, Pin1, and HA antibodies (*upper panel*). Quantitative data are shown in the *lower panel*. *D*, HeLa cells were transfected with Myc-tagged ubiquitin, Oct4, and co-transfected with either empty vector (*EV*) or Pin1. Cells were then treated with MG-132 for 12 h, and lysates were prepared and immunoprecipitated with anti-Myc antibody followed by immunoblotting analysis with anti-Oct4 antibody. Total cell lysates prior to immunoprecipitation (input) were immunoblotted with anti-Pin1 or anti-Oct4 antibody. *E*, human iPS cells were plated on Matrigel-coated feeder-free dishes and treated with either DMSO or juglone (20 μM) for 24 h. Cell lysates were then processed for immunoblotting analysis with anti-Nanog, anti-Oct4, or anti-tubulin antibodies. *F*, a plasmid containing the luciferase (*LUC*) gene flanked with 2601 bp of the Oct4 5′-upstream region was transfected into murine ES cells. The resulting cells were cultured in Matrigel-coated feeder-free dishes and treated with either DMSO or juglone (10 μM) for 24 h, and analyzed by gene reporter assay. *G*, murine ES cells were cultured in Matrigel-coated feeder-free dishes and treated with either DMSO or juglone (10 μM) for 24 h. Total RNAs were then extracted and reverse-transcribed. These preparations were then subjected to quantitative RT-PCR analysis for Oct4. The transcript levels were normalized using GAPDH. *H*, murine ES cells were cultured in Matrigel-coated feeder-free dishes and treated with either DMSO or juglone (10 μM) for 24 h. Cell lysates were then processed for immunoblotting analysis with either anti-Oct4 or anti-β-actin antibody. *I*, HeLa cells were transiently transfected with plasmids encoding Oct4, SOX2, or Pin1 and co-transfected with Oct-SOX reporter gene and pRL-CMV. At 24 h post-transfection, the cells were collected and subjected to a gene reporter assay. *J*, HeLa cells were transiently transfected with an Oct-SOX reporter gene and co-transfected with plasmids encoding wild-type Pin1 or its W34A or K63A mutants, together with Oct4 and SOX2. At 24 h post-transfection, the cells were collected and subjected to a gene reporter assay.

The molecular mechanisms underlying the regulation of Pin1 in the induction and maintenance of pluripotency are likely to be highly complex given that Pin1 interacts with multiple substrates in pluripotent stem cells, as revealed by our proteomics analysis. However, our current findings also indicate that Pin1 is involved in the growth and maintenance of pluripotency in stem cells through its phosphorylation-dependent prolyl isomerization of substrates such as Oct4. In this regard, a recent report by Moretto-Zita *et al.* (30) has demonstrated that Pin1 can also associate with another pluripotent transcription factor, Nanog, in murine ES cells and sustain the self-renewal and teratoma formation of these cells in immunodeficient mice. These results indicate that Pin1 is a crucial modulator of the transcription factor network governing cellular stemness. It is possible also that Pin1 could regulate this process by modulating the function of other substrates. Further studies of Pin1 function in stem cells at various stages might shed new light on the underlying molecular pathways and factors that control self-renewal and multipotency.

It has been demonstrated that Pin1 knock-out mice develop normally but display some proliferation abnormalities, including a decreased body weight, retinal degeneration, and impaired mammary gland development (31, 32). Pin1 knock-out mice also exhibit testicular atrophy with a significantly impaired proliferation of primordial germ cells and the progressive loss of spermatogenic cells (33). These phenotypes can now be attributed to the impaired maintenance and proliferation of germ-related stem cells due to the loss of Pin1 function.

In many circumstances, Pin1 acts as either a repressor or an enhancer of the degradation of substrate proteins (15–17, 34). Our current data now additionally demonstrate that Pin1 can also prolong the protein half-life of Oct4, thereby enhancing its transcriptional activity. Oct4 has been shown to be regulated by post-translational modifications such as SUMOlylation (35). Our current findings reveal that Oct4 is also regulated by phosphorylation and subsequent prolyl isomerization. Identification of the kinase(s) responsible for the association of Pin1 and Oct4 will enhance our understanding of the regulatory pathways that operate during and after the induction of pluripotency.

It is desirable to utilize pluripotent stem cells such as iPS cells for future regenerative medicine applications. However, there are already concerns surrounding the use of iPS cells in a clinical setting because prior studies have suggested that they are likely to develop cancers (4, 36). Our current findings suggest, however, that the Pin1 inhibition could effectively block the proliferation of iPS cells in an undifferentiated state. Pin1 could therefore act as a molecular switch that can reversibly control the proliferation and survival of iPS cells, thereby reducing the risk of cell transformation and tumor formation.

Acknowledgments—We are grateful to the Riken Bioresource Center for providing human iPS cells and MRC5 fibroblasts. We also thank M. Machida, A. Hosoda, and S. Yoshizaki for comments on the manuscript and critical discussions and S. Baba and T. Taniguchi for technical assistance.

REFERENCES

1. Thomson, J. A., Itskovitz-Eldor, J., Shapiro, S. S., Waknitz, M. A., Swiergiel, J. J., Marshall, V. S., and Jones, J. M. (1998) *Science* **282,** 1145–1147
2. Watt, F. M., and Hogan, B. L. (2000) *Science* **287,** 1427–1430
3. Lewitzky, M., and Yamanaka, S. (2007) *Curr. Opin. Biotechnol.* **18,** 467–473
4. Takahashi, K., and Yamanaka, S. (2006) *Cell* **126,** 663–676
5. Boyer, L. A., Lee, T. I., Cole, M. F., Johnstone, S. E., Levine, S. S., Zucker, J. P., Guenther, M. G., Kumar, R. M., Murray, H. L., Jenner, R. G., Gifford, D. K., Melton, D. A., Jaenisch, R., and Young, R. A. (2005) *Cell* **122,** 947–956
6. Eiselleova, L., Matulka, K., Kriz, V., Kunova, M., Schmidtova, Z., Neradil, J., Tichy, B., Dvorakova, D., Pospisilova, S., Hampl, A., and Dvorak, P. (2009) *Stem Cells* **27,** 1847–1857
7. Dvorak, P., Dvorakova, D., Koskova, S., Vodinska, M., Najvirtova, M., Krekac, D., and Hampl, A. (2005) *Stem Cells* **23,** 1200–1211
8. Li, J., Wang, G., Wang, C., Zhao, Y., Zhang, H., Tan, Z., Song, Z., Ding, M., and Deng, H. (2007) *Differentiation* **75,** 299–307
9. Sun, H., and Tonks, N. K. (1994) *Trends Biochem. Sci.* **19,** 480–485
10. Brill, L. M., Xiong, W., Lee, K. B., Ficarro, S. B., Crain, A., Xu, Y., Terskikh, A., Snyder, E. Y., and Ding, S. (2009) *Cell Stem Cell* **5,** 204–213
11. Prudhomme, W., Daley, G. Q., Zandstra, P., and Lauffenburger, D. A. (2004) *Proc. Natl. Acad. Sci. U.S.A.* **101,** 2900–2905
12. Hunter, T. (2009) *Curr. Opin. Cell Biol.* **21,** 140–146
13. Lu, K. P., Hanes, S. D., and Hunter, T. (1996) *Nature* **380,** 544–547
14. Ryo, A., Liou, Y. C., Lu, K. P., and Wulf, G. (2003) *J. Cell Sci.* **116,** 773–783
15. Ryo, A., Suizu, F., Yoshida, Y., Perrem, K., Liou, Y. C., Wulf, G., Rottapel, R., Yamaoka, S., and Lu, K. P. (2003) *Mol. Cell* **12,** 1413–1426
16. Ryo, A., Nakamura, M., Wulf, G., Liou, Y. C., and Lu, K. P. (2001) *Nat. Cell Biol.* **3,** 793–801
17. Lu, K. P., and Zhou, X. Z. (2007) *Nat. Rev. Mol. Cell Biol.* **8,** 904–916
18. Esnault, S., Shen, Z. J., and Malter, J. S. (2008) *Crit. Rev. Immunol.* **28,** 45–60
19. Takahashi, K., Okita, K., Nakagawa, M., and Yamanaka, S. (2007) *Nat. Protoc.* **2,** 3081–3089
20. Yamada, M., Hamatani, T., Akutsu, H., Chikazawa, N., Kuji, N., Yoshimura, Y., and Umezawa, A. (2010) *Hum. Mol. Genet.* **19,** 480–493
21. Liu, Y., and Labosky, P. A. (2008) *Stem Cells* **26,** 2475–2484
22. Masui, S., Nakatake, Y., Toyooka, Y., Shimosato, D., Yagi, R., Takahashi, K., Okochi, H., Okuda, A., Matoba, R., Sharov, A. A., Ko, M. S., and Niwa, H. (2007) *Nat. Cell Biol.* **9,** 625–635
23. Yang, H. M., Do, H. J., Oh, J. H., Kim, J. H., Choi, S. Y., Cha, K. Y., Chung, H. M., and Kim, J. H. (2005) *J. Cell. Biochem.* **96,** 821–830
24. Takahashi, K., Ichisaka, T., and Yamanaka, S. (2006) *Methods Mol. Biol.* **329,** 449–458
25. Hennig, L., Christner, C., Kipping, M., Schelbert, B., Rücknagel, K. P., Grabley, S., Küllertz, G., and Fischer, G. (1998) *Biochemistry* **37,** 5953–5960
26. Shen, Z. J., Esnault, S., Schinzel, A., Borner, C., and Malter, J. S. (2009) *Nat. Immunol.* **10,** 257–265
27. Yaffe, M. B., Schutkowski, M., Shen, M., Zhou, X. Z., Stukenberg, P. T., Rahfeld, J. U., Xu, J., Kuang, J., Kirschner, M. W., Fischer, G., Cantley, L. C., and Lu, K. P. (1997) *Science* **278,** 1957–1960
28. Lu, P. J., Zhou, X. Z., Liou, Y. C., Noel, J. P., and Lu, K. P. (2002) *J. Biol. Chem.* **277,** 2381–2384
29. Niwa, H., Miyazaki, J., and Smith, A. G. (2000) *Nat. Genet.* **24,** 372–376
30. Moretto-Zita, M., Jin, H., Shen, Z., Zhao, T., Briggs, S. P., and Xu, Y. (2010) *Proc. Natl. Acad. Sci. U.S.A.* **107,** 13312–13317
31. Fujimori, F., Takahashi, K., Uchida, C., and Uchida, T. (1999) *Biochem. Biophys. Res. Commun.* **265,** 658–663
32. Liou, Y. C., Ryo, A., Huang, H. K., Lu, P. J., Bronson, R., Fujimori, F., Uchida, T., Hunter, T., and Lu, K. P. (2002) *Proc. Natl. Acad. Sci. U.S.A.* **99,** 1335–1340
33. Atchison, F. W., and Means, A. R. (2003) *Biol. Reprod.* **69,** 1989–1997
34. Ryo, A., Hirai, A., Nishi, M., Liou, Y. C., Perrem, K., Lin, S. C., Hirano, H., Lee, S. W., and Aoki, I. (2007) *J. Biol. Chem.* **282,** 36671–36681
35. Zhang, Z., Liao, B., Xu, M., and Jin, Y. (2007) *FASEB J.* **21,** 3042–3051
36. Knoepfler, P. S. (2009) *Stem Cells* **27,** 1050–1056

Laboratory Investigation (2011) 91, 553–564

Coronary vein infusion of multipotent stromal cells from bone marrow preserves cardiac function in swine ischemic cardiomyopathy via enhanced neovascularization

Takatoshi Sato[1,*], Yoshitaka Iso[2,*], Taro Uyama[3], Keisuke Kawachi[2], Kohei Wakabayashi[2], Yasutoshi Omori[1], Teruko Soda[1], Makoto Shoji[1], Shinji Koba[1], Shin-Ichiro Yokoyama[4], Noboru Fukuda[5], Satoshi Saito[4], Takashi Katagiri[1], Youichi Kobayashi[1], Youichi Takeyama[2], Akihiro Umezawa[3] and Hiroshi Suzuki[2]

Few reports have examined the effects of adult bone marrow multipotent stromal cells (MSCs) on large animals, and no useful method has been established for MSC implantation. In this study, we investigate the effects of MSC infusion from the coronary vein in a swine model of chronic myocardial infarction (MI). MI was induced in domestic swine by placing beads in the left coronary artery. Bone marrow cells were aspirated and then cultured to isolate the MSCs. At 4 weeks after MI, MSCs labeled with dye ($n=8$) or vehicle ($n=5$) were infused retrogradely from the anterior interventricular vein without any complications. Left ventriculography (LVG) was performed just before and at 4 weeks after cell infusion. The ejection fraction (EF) assessed by LVG significantly decreased from baseline up to a follow-up at 4 weeks in the control group ($P<0.05$), whereas the cardiac function was preserved in the MSC group. The difference in the EF between baseline and follow-up was significantly greater in the MSC group than in the control group ($P<0.05$). The MSC administration significantly promoted neovascularization in the border areas compared with the controls ($P<0.0005$), though it had no affect on cardiac fibrosis. A few MSCs expressed von Willebrand factor in a differentiation assay, but none of them expressed troponin T. In quantitative gene expression analysis, basic fibroblast growth factor and vascular endothelial growth factor (VEGF) levels were significantly higher in the MSC-treated hearts than in the controls ($P<0.05$, respectively). Immunohistochemical staining revealed VEGF production in the engrafted MSCs. *In vitro* experiment demonstrated that MSCs significantly stimulated endothelial capillary network formation compared with the VEGF protein ($P<0.0001$). MSC infusion via the coronary vein prevented the progression of cardiac dysfunction in chronic MI. This favorable effect appeared to derive not from cell differentiation, but from enhanced neovascularization by angiogenic factors secreted from the MSCs.
Laboratory Investigation (2011) **91,** 553–564; doi:10.1038/labinvest.2010.202; published online 31 January 2011

KEYWORDS: angiogenesis; bone marrow; chronic myocardial infarction; coronary vein; multipotent stromal cells

In recent years, cell-based therapy has emerged as a potential new strategy for organ repair. The optimal source of cells for repairing damaged tissue is a topic of intense research. Bone marrow mononuclear cells (BMNCs) have been the cell source most frequently used for the angiogenic cell therapies applied for cardiovascular disease.[1–5] Two randomized controlled trials in Europe, however, failed to prove any functional benefit of intracoronary applied BMNCs in patients with acute myocardial infarction (MI).[4,5] The results of these trials suggest that the effects of BMNC implantation may be

[1]Division of Cardiology, Department of Medicine, Showa University School of Medicine, Tokyo, Japan; [2]Division of Cardiology, Department of Internal Medicine, Showa University Fujigaoka Hospital, Yokohama, Japan; [3]Department of Reproductive Biology and Pathology, National Research Institute for Child Health and Development, Tokyo, Japan; [4]Division of Cardiology, Department of Medicine, Nihon University School of Medicine, Tokyo, Japan and [5]Advanced Research Institute of the Sciences and Humanities, Nihon University, Tokyo, Japan
Correspondence: Dr H Suzuki, MD, PhD, Division of Cardiology, Department of Internal Medicine, Showa University Fujigaoka Hospital, 1–30 Fujigaoka, Aoba-ku, Yokohama, Kanagawa 227-8501, Japan.
E-mail: hrsuzuki@med.showa-u.ac.jp
*These authors contributed equally to this work.

Received 11 February 2010; revised 1 November 2010; accepted 11 November 2010

insufficient to improve cardiac function. A new cell therapy using other cell types, a therapy more effective than BMNC implantation, is expected to be established soon.

Our group previously demonstrated the important contributions of the stem/progenitor cells among the BMNCs in improving limb ischemia.[6] There has been considerable interest in the development of a new therapy with a non-hematopoietic subset of adult bone marrow (BM) stem/progenitor cells referred to as the mesenchymal stem cells or multipotent stromal cells (MSCs) in cardiac repair or regeneration.[7–11] MSCs have been shown to protect against ischemic injury through both direct prevention of cell death and through the stimulation of angiogenesis.[7,11] In experiments comparing cultured human MSCs with BM hematopoietic stem/progenitor cells, Iso *et al*[7] found that the former expressed higher mRNA levels for angiogenic factors such as vascular endothelial growth factor (VEGF) and adrenomedullin. Encouragingly, translational studies on small and large models toward clinical implication have shown that MSC administration in the acute phase of MI improves cardiac function.[8,9,12–14] It remains undetermined, however, whether MSC implantation is effective in a chronic MI or heart failure model.

As the selection of cell types advances, methods and devices for cell delivery will also have to be developed for clinical cell therapies. The methods used for cell implantation have included direct injection into myocardium after thoracotomy,[14] transendocardial injection via an injection catheter,[8] and intracoronary injection via a balloon catheter.[9] The first of these methods, via thoracotomy, poses an increased risk of morbidity and mortality, as it requires highly aggressive intervention and general anesthesia. The second method, transendocardial injection with a catheter, also has flaws, including risks such as cardiac tamponade and ventricular arrhythmia. As hopeful alternatives, new methods of cell transplantation have recently been reported.[15–18] We previously demonstrated the safety and efficacy of retrograde injection of BMNCs via the coronary vein into the myocardium through a single balloon infusion catheter in a swine MI model.[15]

Our group conducted this study for two purposes: first, to investigate whether the low invasive delivery of MSCs via the coronary vein restores cardiac function in chronic ischemic cardiomyopathy model; second, to explore the mechanism behind the improvement, if any improvement is found.

MATERIALS AND METHODS

Isolation of Swine MSCs

This study was conducted according to the Guide for the Care and Use of Laboratory Animals published by the United States National Institutes of Health. The experimental protocol was approved by the Animal Care and Use Committee of Showa University School of Medicine.

Swine BM cells were harvested from the femurs of the swine as the MI model was being created (Figure 1a). These

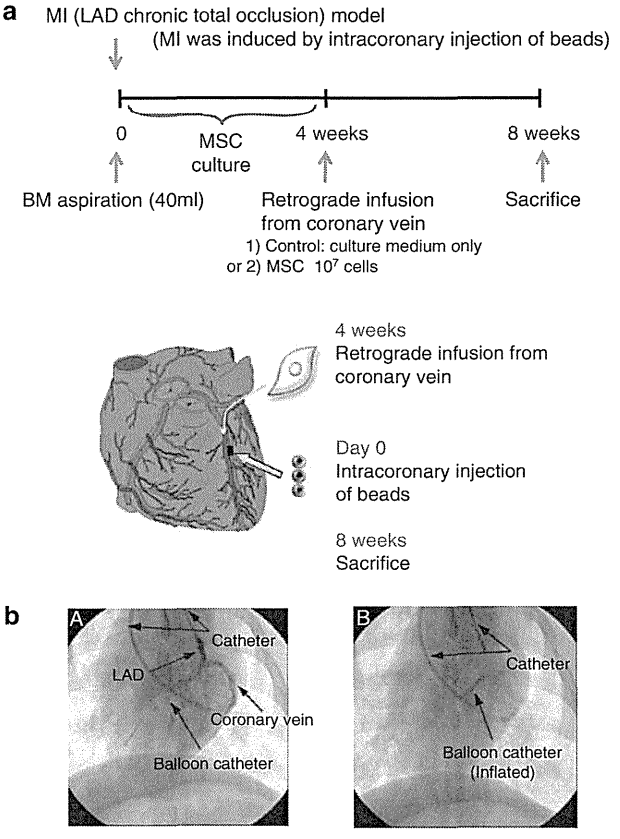

Figure 1 Experimental protocol and procedure. (**a**) Schedule and scheme for the experimental protocol. (**b**) Left coronary angiography and coronary venography (left), and X-ray image at balloon inflation with cell infusion (right). MI, myocardial infarction. BM, bone marrow. MSC, multipotent stromal cell.

cells were resuspended in MSC culture medium (10% fetal bovine serum in Dulbecco's modified Eagle's medium containing 4.5 g/l glucose) with antibiotic/antimycotic supplements (Invitrogen, Carlsbad, CA, USA), and the cultures were maintained at 37°C in a humidified atmosphere containing 95% air and 5% CO_2. When the cultures reached subconfluence, the cells were harvested with 0.25% trypsin and 1 mM EDTA, then one-half of the harvested cells were replaced. After one series of passages, the attached MSCs were devoid of hematopoietic cells. After two series of passages, the cells were harvested again with 0.25% trypsin and 1 mM EDTA, washed with phosphate buffer saline, labeled with Celltracker Orange (Invitrogen), and resuspended in 10 ml RPMI Medium 1640 (Invitrogen).

Chronic MI Model and Cell Implantation

In all, 19 male domestic swine, aged 2–4 months and weighing about 25 kg, were used. After receiving an intramuscular injection of ketamine (20 mg/kg) and atropine (60 μg/kg), each animal was intubated, ventilated, and maintained with a mixture of halothane (2%) and oxygen.

Electrocardiograph monitoring was performed continuously, and a coronary angiography was carried out after inserting an introducer from the right cervical artery. Next, the guidewire was inserted into the left anterior descending coronary artery and sterilized beads were placed in the mid left anterior descending coronary artery by microcatheter (Figure 1a and b) according to a method previously described.[15] Peripheral blood was collected before and 1 and 4 days after MI. Serum creatine kinase (CK) levels were determined.

At 4 weeks after the induction of MI by permanent coronary occlusion with the beads, the 13 surviving animals were anesthetized again by the same procedure. After coronary angiography and left ventriculography (LVG), a balloon catheter (2.5 mm in diameter) was advanced through the coronary sinus into the anterior intraventricular vein and positioned just beside the occlusive site of the left anterior descending coronary artery (Figure 1a and c). The swine were randomly assigned to either an MSC infusion group (MSC group: $n=8$) or medium infusion group (control group: $n=5$). In the MSC group, MSCs ($1.02 \pm 0.34 \times 10^7$ cells) labeled with the red fluorescent dye were suspended in 10 ml culture medium and infused retrogradely through the balloon catheter from the anterior intraventricular vein over a 10-min period of balloon inflation. The same volume of medium was infused in the control group by the same procedure.

LVG was performed before and at 4 weeks after the cell implantation to determine cardiac function as previously described.[19] Later, on the completion of follow-up coronary angiography and LVG at 4 weeks after the treatment, the animals were killed and their hearts were harvested. Samples were collected from the infarcted, border, and remote areas in the treated hearts. The tissue was prepared as previously described.[19]

Flow Cytometric Analysis of the Cultured Cells

The characteristics of the cultured MSCs were confirmed by flow cytometric analyses using purified or directly conjugated antibodies against SWC3a (BD PharMingen, San Diego, CA, USA), CD44 (BD PharMingen), SLA-class I (BD PharMingen), CD29 (BD PharMingen), CD44H (FITC-labeled, BD PharMingen), SLA-DQ (BD PharMingen), CD31 (BD PharMingen), and CD90 (PE-labeled; BD PharMingen). The cells were detached and stained for 30 min at 4°C with primary antibodies and immunofluorescent secondary antibodies. After washing, the cells were analyzed on a Cytomics FC500 analyzer (Beckman Coulter, Fullerton, CA, USA).

Immunostaining and Morphometric Analysis

Immunohistochemistry and the morphometric analysis were performed as previously described.[19] The primary antibodies were anti-von Willebrand factor (vWF) for endothelial cells at a 1:400 dilution (Santa Cruz Biotechnology, Santa Cruz, CA, USA), anti-α-smooth muscle actin (SMA) for small arteries at a 1:300 dilution (Sigma, Saint Louis, MO, USA) and phospho-signal transducer and activator of transcription 3 (phospho-STAT3, Cell Signaling Technology, MA, USA) at a 1:50 dilution.

Images of the Mallory-stained sections were recorded, digitized, and analyzed with Win ROOF image analysis software (Mitani, Fukui, Japan) to measure the fibrotic area. The measurements were taken in 10 sections for each animal. To evaluate neovascularization, the numbers of α-SMA- and vWF-positive vessels in the border areas were manually counted in a randomly selected high-power field (× 400). The measurements were taken in 10 areas for each animal. The investigator performing this analysis was blinded to the treatment.

Immunofluorescence

Before staining, frozen sections were fixed for 10 min in chloroform at room temperature. The sections were incubated with the first antibody: either anti-vWF antibody (Santa Cruz Biotechnology) at a 1:300 dilution for 60 min at room temperature, or anti-troponin T antibody (Neo-Markers, Fremont, CA, USA) at a 1:100 dilution for 60 min at room temperature, or anti-VEGF antibody (Santa Cruz Biotechnology) at a 1:800 dilution for 24 h at 4°C. After incubation with the first antibody, the sections were incubated with the second antibody: Alexa 488-labeled IgG (green color; Molecular Probes, Eugene, OR, USA; 1:400 dilution) for 1 h. Nuclear staining was performed by DAPI.

Quantitative mRNA Expression Analysis for Basic Fibroblast Growth Factor (bFGF) and VEGF

An RNA extraction, reverse transcription-polymerase chain reaction (RT-PCR) analysis and quantification of the PCR products were performed as previously described.[19] The PCR primers were as follows: bFGF, forward 5′-TCAAAG GAGTGTGTGCGAAC-3′ and reverse 5′-CAGGGCCACATA CCAACTG-3′; VEGF, forward 5′-ATGCGGATCAAACC TCACC-3′ and reverse 5′-ATCTGGTTCCCGAAACGCTG-3′; GAPDH, forward 5′-TCACCATCTTCCAGGAGCGA-3′ and reverse 5′-CACAATGCCGAAGTGGTCGT-3′. PCR reactions were carried out as follows: for bFGF, 35 cycles of denaturation for 60 s at 94°C, annealing for 45 s at 59°C, and extension for 45 s at 72°C; for VEGF, 27 cycles of denaturation for 30 s at 94°C, annealing for 1 min at 60°C, and extension for 2 min at 68°C, followed by a final extension for 7 min at 68°C; for GAPDH, 30 cycles of denaturation for 1 min at 94°C, annealing for 90 s at 55°C, and extension for 2 min at 72°C.

The sizes and quantities of the PCR products were detected by an Agilent 2100 Bioanalyzer (Agilent Technologies, CA, USA) according to the manufacturer's instructions. In brief, 9 ml of gel-dye mix was fed into each of 16 wells and then forced into a micro channel network. Each of two buffer wells was also filled with 9 ml of the gel-dye mix, and sample and ladder wells were filled with 5 ml of marker mix followed by 1 ml of DNA sizing ladder and sample, respectively. The

prepared microchip was vortexed and placed into the bioanalyzer for analysis. All experiments were performed using Agilent biosizing software (Version A.02.12).

Immunoblotting

The immunoblotting was performed by a method previously described,[20] with minor modifications. A total of 20 μg of protein was separated by SDS-PAGE. The protein was transferred from gel to a clear blot P membrane sheet (Atto, Tokyo, Japan) by horizontal electrophoresis at 108 mA for 90 min at room temperature. Immunostaining was carried out with anti-VEGF (Santa Cruz Biotechnology) and bFGF (Millipore, CA, USA) antibodies.

In Vitro Angiogenesis Assay

Tubule formation experiments were conducted using an Angiogenesis kit (Kurabo, Osaka, Japan), according to the manufacturer's instructions. Briefly, human umbilical vein

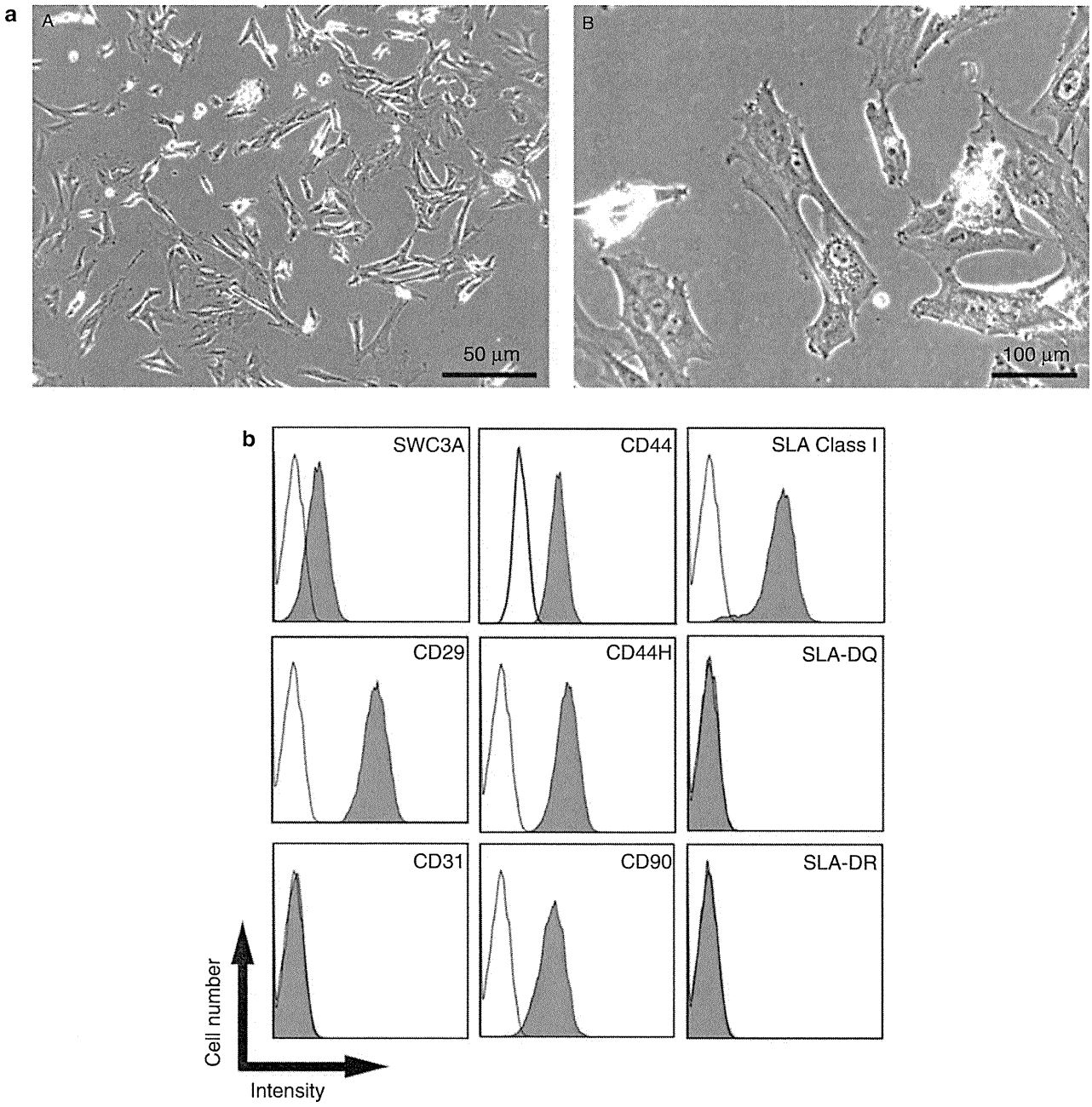

Figure 2 Phenotype of swine MSCs. (**a**) Phase contrast microscopic images of MSCs (A, low magnification; B, high magnification). (**b**) Flow cytometric analysis of swine MSCs. MSCs are positive for SWC3a, CD44, SLA class I, CD29, CD44H, and CD90, and negative for SLA-DQ, CD31, and SLA-DR.

endothelial cells (HUVECs) and human fibroblasts were admixed and seeded into 24-well plates. Human MSCs (5×10^4 cells/well) were applied and co-cultured for the experiments. After 10 days of culture, the HUVECs were fixed with 70% ethanol at 4°C and immunostained with an anti-human CD31 antibody using BCIP/NBT as a substrate for the secondary antibody. Five fields per well were selected for digital photography under a microscope (Olympus, Tokyo, Japan), and the areas of the tubule-like structures were measured quantitatively using angiogenesis image analyzer software (Kurabo).

Statistical Analysis

All values are expressed as means ± s.e.m. The means were compared by the unpaired Student's *t*-test. The paired *t*-test was used for comparison of temporal changes in the ejection fraction (EF). Comparisons among the three groups were conducted by one-way analysis of variance followed by Scheffé's multiple comparison test. A *P*-value of <0.05 was considered statistically significant.

RESULTS

Phenotype of Swine MSCs

Bone marrow was aspirated from the swine femurs as the MI model was being created (Figure 1a). The mononuclear cell layer from the BM was cultured, and the MSCs adhering to the culture plastic after 24–48 h were isolated. The cultured swine MSCs were phenotypically similar to human MSCs. They had a fibroblastic spindle-like shape typical of mesenchymal cells and were positive for CD44, SLA class I, CD29, and CD90, and negative for CD31 (Figure 2).

Cardiac Function in Chronic MI after the MSC Implantation

We measured the serum CK levels to assess acute myocardial damage after the sterilized beads were implanted in the swine LADs. The levels of CK peaked at 1 day after the infarction, and the peak levels were similar in the two groups (3338.6 ± 538.5 mg/dl in the control group, 3447.7 ± 561.7 mg/dl in the MSC group).

At 4 weeks after the MI, the swine were treated with the MSCs ($1.02 \pm 0.34 \times 10^7$ cells, $n=8$) or vehicle ($n=5$) via coronary vein infusion (Figure 1c). Coronary venography confirmed that the vessels were free of complications such as vein rupture or embolization during the procedure. To determine cardiac function, LVG was performed immediately before and at 4 weeks after the treatment. The EF assessed by the LVG did not significantly differ between the two groups at baseline. The EF significantly decreased in the

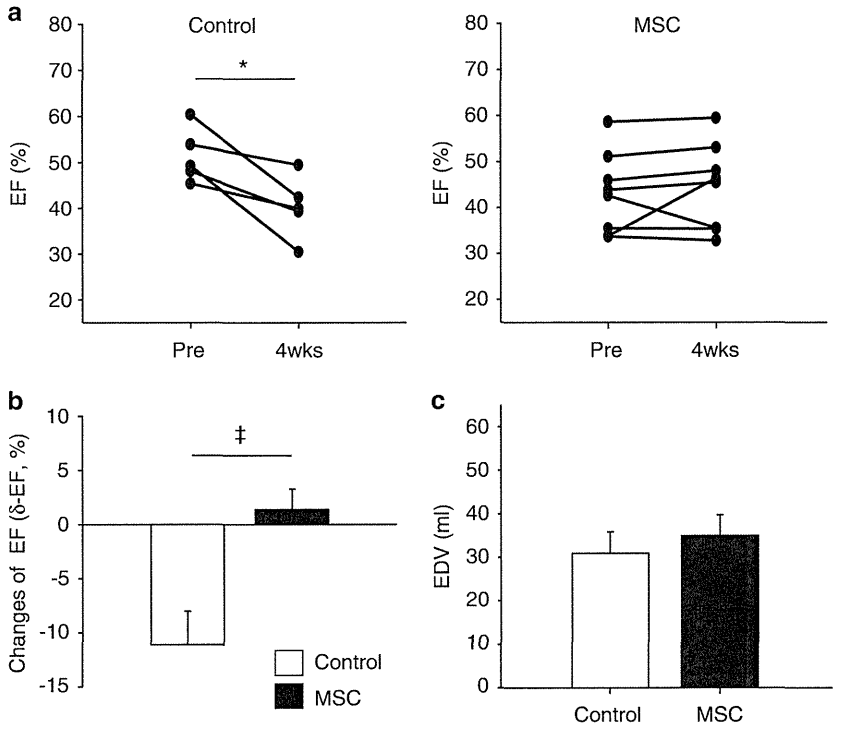

Figure 3 Cardiac function assessed by left ventriculography. (**a**) Time course changes in ejection fraction (EF) immediately before and at 4 weeks after treatment. Left, control group ($n=5$); right, MSC infusion group ($n=8$). (**b**) Differences between pre-treatment EF and EF after 4 weeks (δ-EF). (**c**) Endodiastolic volumes at 4 weeks after treatment. No significant differences between the two groups were observed. Data are means ± s.e.m.*$P<0.05$; ‡$P<0.01$.

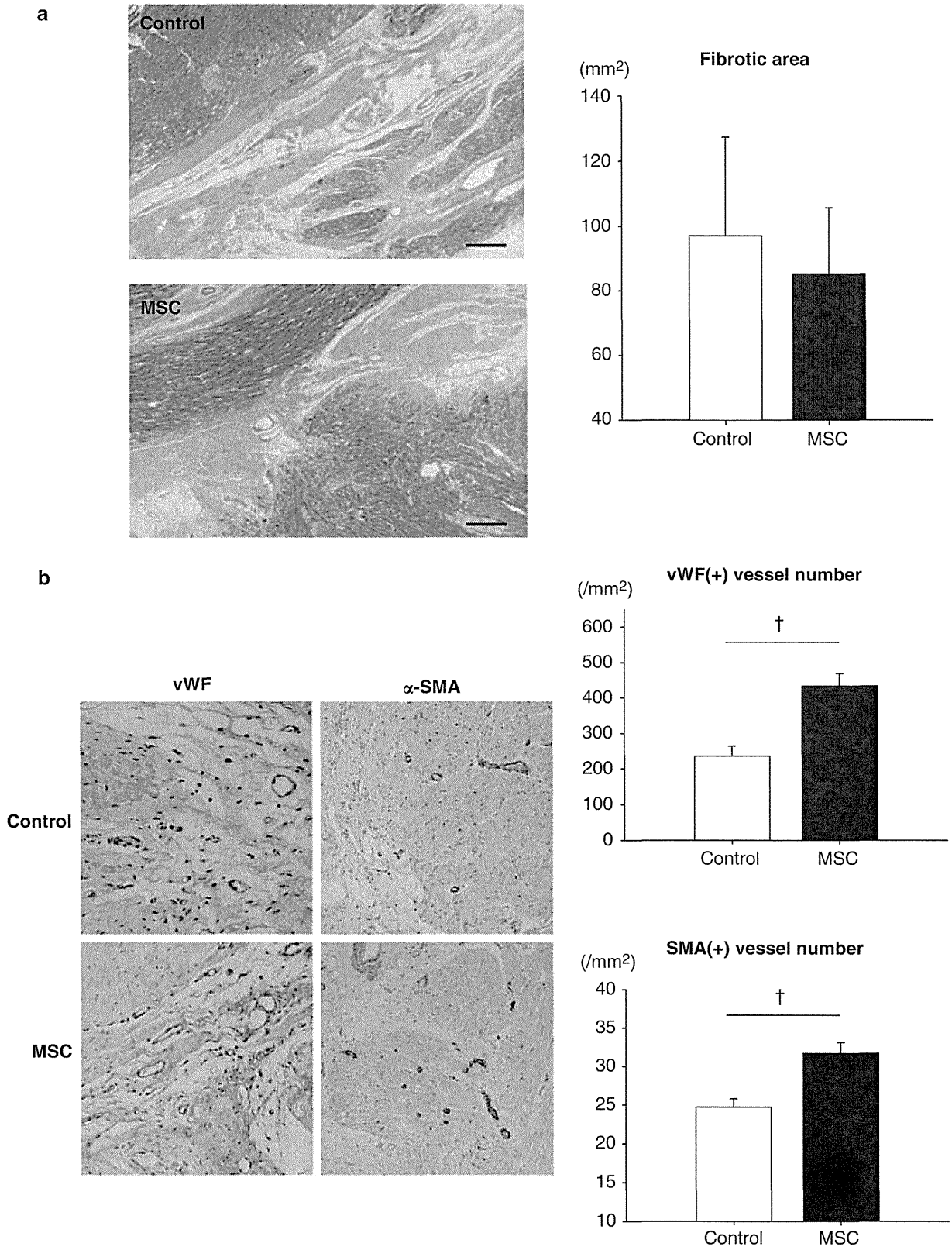

Figure 4 Cardiac fibrosis and neovascularization in hearts after cell infusion. (**a**) Left, blue staining indicates fibrosis in the Azan-Mallory-stained sections. Right, the morphometric analysis shows no significant differences in the fibrotic area between the two groups. (**b**) Left, neovessels are evaluated in the von Willebrand factor (vWF)- and the α-smooth muscle actin (α-SMA)-stained sections. Right, the numbers of vWF- and α-SMA-positive vessels in the border areas. Data are means ± s.e.m. $^{\dagger}P<0.0005$.

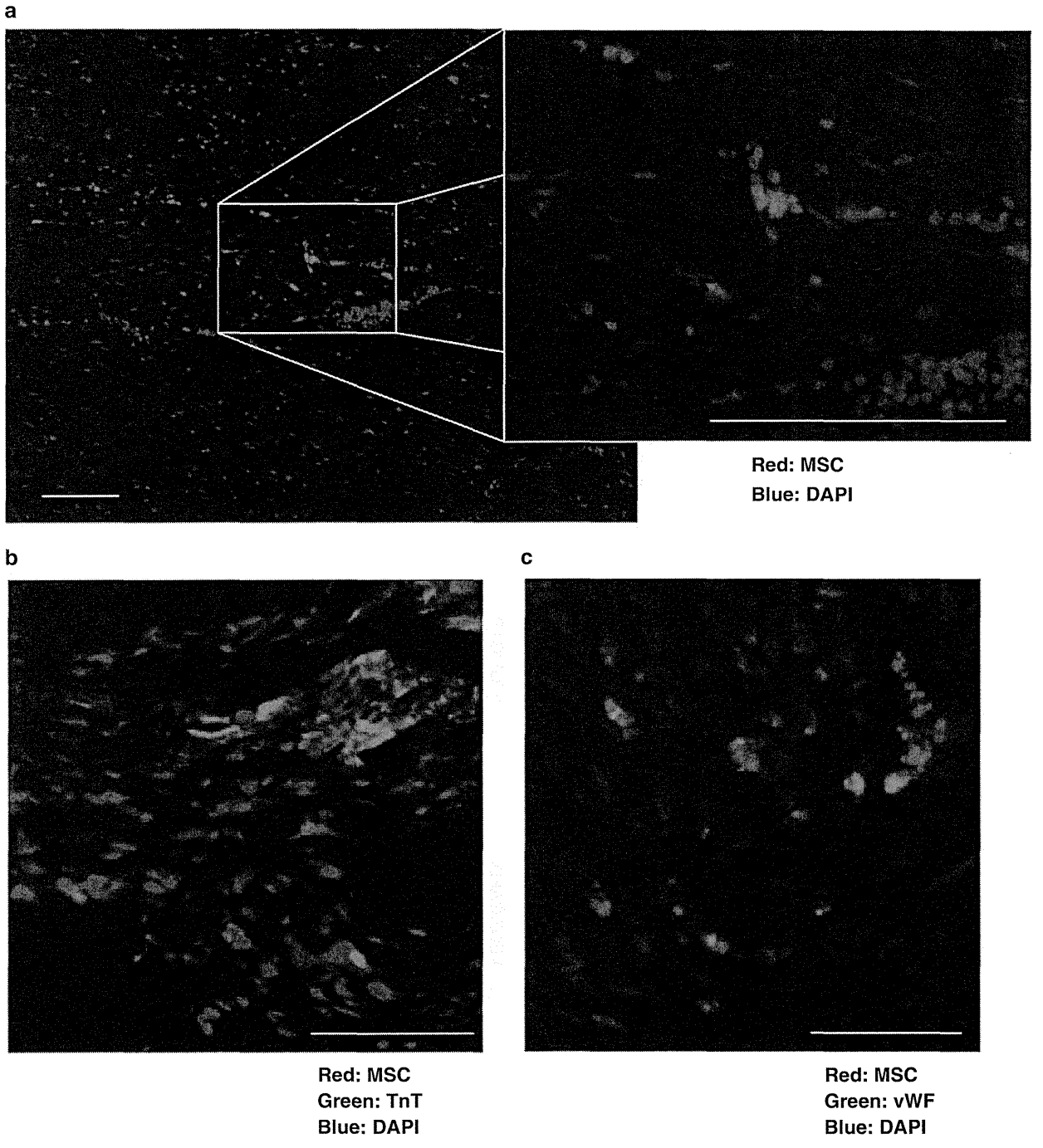

Figure 5 MSC engraftment and differentiation. (**a**) Engraftment of MSCs implanted in the border area. Red fluorescence indicates MSCs. Blue fluorescence indicates DAPI nuclear staining. (**b**) Lack of cardiomyocyte differentiation of the engrafted MSCs. Implanted Red fluorescence indicates MSCs. Green fluorescence indicates myocardium (TnT = troponin T). Blue fluorescence indicates DAPI nuclear staining. (**c**) Endothelial cell differentiation of the engrafted MSCs. Red fluorescence indicates MSCs. Green fluorescence indicates endothelial cells (vWF). Yellow (red and green) fluorescence indicates MSC differentiation. Blue fluorescence indicates DAPI nuclear staining. Bar = 100 μm.

control group over time ($P<0.05$), whereas the cardiac function was preserved in the MSC group (Figure 3a). The difference in the EF (δ-EF) between the baseline and follow-up was significantly smaller in the controls than in the MSC animals ($P<0.01$, Figure 3b). There were no statistically significant differences between the two groups in the EF or end-diastolic volume at follow-up (Figure 3c).

These findings from the LVG studies indicate that retrograde delivery of the MSCs via the coronary vein suppresses the progression of systolic LV dysfunction in chronic MI.

Effects of the Cell Infusion on Cardiac Fibrosis and Neovascularization

We conducted histopathological studies to address the effects of the MSC administration on cardiac fibrosis and neovascularization. Azan-Mallory-stained sections of hearts from the MSC-treated swine showed somewhat less fibrosis than those from the controls, but the difference was not significant in quantitative analysis (Figure 4a). The numbers of vWF- and α-SMA-positive vessels were assessed in the border areas (Figure 4b). The number of vWF-positive vessels was significantly higher in the MSC-treated swine hearts than in the control group ($P<0.0005$). Likewise, α-SMA-positive vessel counts were also significantly higher in the MSC group than in the control group ($P<0.0005$).

The effects of the MSC infusion were limited in terms of modification of cardiac fibrosis in the chronic post-infarcted myocardium, while the cell administration significantly promoted angio/arteriogenesis in the border zones. Thus, the favorable effects of the MSCs on cardiac function appeared to derive, at least in part, from enhanced neovascularization.

In a previous report from another group,[21] freshly isolated BM cell implantation induced a calcified lesion formation in the infarcted myocardium of rat. Noting this, we carried von Kossa staining to detect abnormal calcium deposition in the frozen sections. This staining, however, revealed no calcified lesions (data not shown).

Engraftment and Differentiation of the Implanted MSCs

We assessed MSC engraftment and differentiation by immunofluorescence. MSCs marked by red fluorescence dye were sparsely observed in an interstitial area of the border area at 4 weeks after the infusion, but we could not detect any cells differentiated to cardiomyocytes (Figure 5a and b). A few MSCs expressed vWF and were incorporated into the vessel structure (Figure 5c).

The effect of the engrafted MSCs in promoting neovascularization seemed to be conferred partly through endothelial differentiation. The extent of the differentiation, however, was far too low to account for the significant increases in the vessel numbers.

Enhanced Expression of Angiogenic Factors after the MSC Implantation

Noting the reduced extent of cell incorporation to neovessels, we examined whether factors related to angiogenesis contributed to the increased neovascularization in the treated myocardium.

We determined the gene expression levels of bFGF and VEGF relative to GAPDH by quantitative RT-PCR analysis. The bFGF and VEGF levels were significantly higher in the MSC-treated hearts than in the control hearts ($P<0.05$, respectively; Figure 6a). Immunoblotting analysis confirmed the increased protein expressions of both bFGF and VEGF in the MSC group compared with the controls (Figure 6b). Of note, the MSC infusion enhanced the transcriptional levels not only in the border and infarcted areas, but also in the remote areas with little to no MSC engraftment (Figure 6a). In response to the MSC infusion, resident cardiac cells in the remote areas appeared to produce these angiogenic cytokines.

Immunohistochemical staining revealed that the MSCs engrafted in the border zones produced VEGF (Figure 7a).

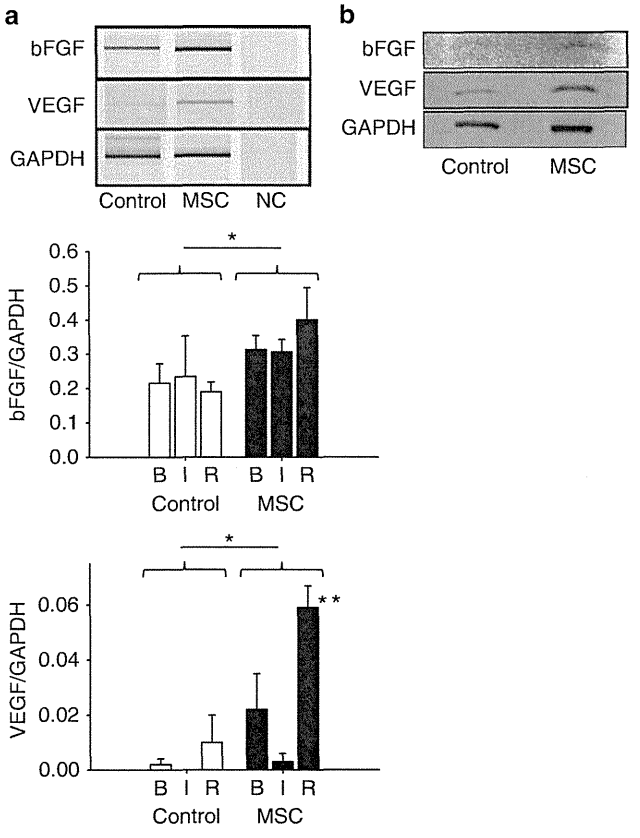

Figure 6 Expressions of bFGF and VEGF in the hearts after cell infusion. (**a**) Representative images of electrophoretic gels after PCR amplification of FGF and VEGF mRNA in the border areas (upper). Quantitative analysis of bFGF mRNA expression relative to GAPDH mRNA in each area of the heart (middle). Quantitative analysis of VEGF mRNA expression relative to GAPDH mRNA in each area of the heart (bottom). Data are means ± s.e.m., $n=3$ in each area. $^{*}P<0.05$. $^{**}P<0.05$ *vs* infarcted area in the MSC group. B, border area. I, infarcted area. R, remote area. (**b**) Immunoblotting analysis for bFGF and VEGF protein expressions in the border area. bFGF, basic fibroblast growth factor. VEGF, vascular endothelial growth factor.

Figure 7 Expressions of VEGF and pro-angiogenic signal in the MSC-treated hearts. (**a**) VEGF production from the engrafted MSCs. Red fluorescence indicates MSCs. Green fluorescence indicates VEGF. Blue fluorescence indicates DAPI nuclear staining. Merged image (yellow fluorescence) shows VEGF expression in the MSCs. Bar = 20 μm. (**b**) STAT3 activation in the resident cardiac cells. Left, MSC engraftment (red fluorescence and white arrow). Blue fluorescence indicates DAPI nuclear staining. Right, clusters of cardiac cells with activated STAT3. Brown indicates positive staining for phospho-STAT3. Bar = 50 μm. STAT3, signal transducer and activator of transcription 3.

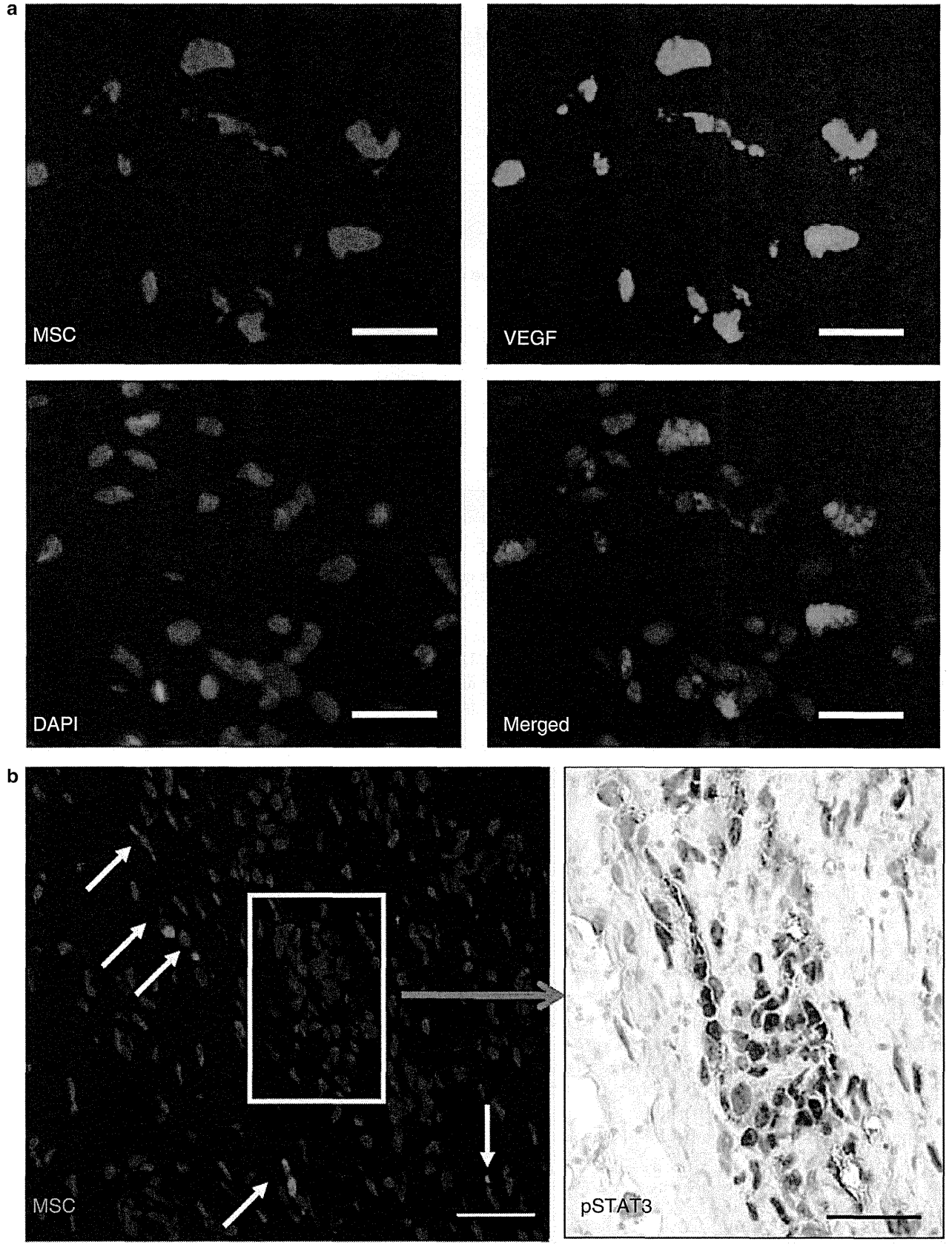
a
MSC
VEGF
DAPI
Merged
b
MSC
pSTAT3

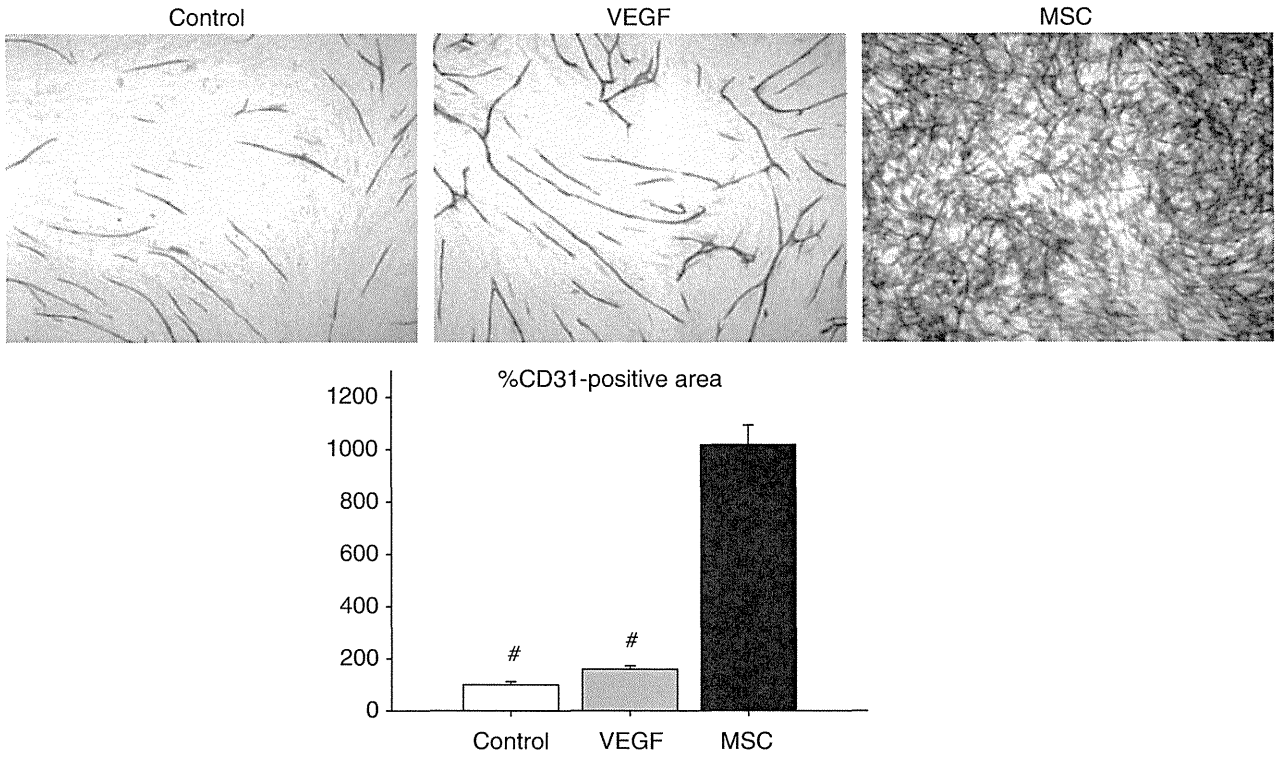

Figure 8 *In vitro* angiogenesis assay. Comparison of %CD31 areas among the growth medium (100%), the growth medium supplemented with VEGF 10 ng/ml, and the MSC co-culture. Data are means ± s.e.m., $n = 3$–4. $^{\#}P < 0.0001$ *vs* MSC.

MSCs have been shown to secrete IL-6 and leukemia inhibitory factor.[7,22] The transcriptional factor STAT3 is activated by IL-6 family members, and its activation promotes capillary growth in adult heart via acceleration of VEGF transcription.[23] We found that the area surrounded by the engrafted MSCs contained clusters of cells positive for phosphorylated + -STAT3 in sequential sections of the swine infarcted myocardium (Figure 7b).

Thus, VEGF might be produced not only the MSCs, but also by resident cardiac cells with STAT3 activated by the MSC-secreted factors.

In Vitro Angiogenesis Assay

We examined the culture system by an angiogenesis assay. HUVECs were immunostained with an anti-CD31 antibody, and the colored areas were quantified as capillary growth. Co-culture with human MSCs (5×10^4 cells) prominently induced the capillary network formation (Figure 8). The capillary area was significantly larger in the MSCs than in the control medium or the control medium supplemented with a high concentration (10 ng/ml) of VEGF ($P < 0.0001$, respectively).

DISCUSSION

Various reports have demonstrated a potential relationship between cardiac angiogenesis and cardiac function.[24–26] Disruption of the balance between myocyte growth and angiogenesis leads to contractile dysfunction and heart failure. VEGF plays a critical role in this process.

In an earlier study by our group, BMNCs implanted via the coronary vein improved cardiac function in the acute and subacute phase of MI.[15] MSCs have been shown to be a robust source of angiogenic factors compared with hematopoietic cells in BM.[7,27] The low-invasive local delivery of MSCs preserved cardiac function in the swine chronic MI model in our present study. In comparisons against our controls, swine hearts implanted with MSCs exhibited increased expression of VEGF and bFGF and larger numbers of vessels in vWF and α-SMA staining. The enhanced neovascularization induced by the increased VEGF may help to prevent the progression of cardiac dysfunction in the chronic MI model.

Immunohistochemical staining revealed that the elevated VEGF levels were at least partly due to VEGF release from the engrafted MSCs. MSCs significantly promoted capillary network formation in our endothelial tube formation assay *in vitro*. The results of this *in vitro* study may support the hypothesis that factors secreted by the MSCs *in vivo* are responsible for enhanced neovascularization and preserved contractile function. Several previous studies support the paracrine hypothesis for MSC-mediated angiogenesis and cardioprotection.[7,11,27,28] Moreover, our RT-PCR analysis showed significant increases in the VEGF levels in the remote

areas wholly devoid of MSCs. The MSC-treated heart contained clusters of resident cells positive for phospho-STAT3, the regulator of VEGF production. Human MSCs expressed higher mRNA levels of both VEGF and IL-6 family members than the human BM CD133+ progenitors, and secreted those factors *in vitro*.[7] On this basis, we speculate that MSC-secreted factors, such as VEGF and IL-6, promote neovascularization both directly through endothelial proliferation and indirectly through activation of STAT3 in the resident cells.

Our previous study demonstrated that the safety and feasibility of the cell delivery via the coronary vein in a preclinical trial with the pig models.[15] For the reasons explained below, we also selected coronary vein infusion as the route for MSC delivery into the myocardium in the present study. We did not, however, compare it with the other delivery methods (eg, intracoronary infusion and intramyocardial injection) in our hands. Intracoronary infusion of MSCs may cause distal embolization and consequent no-reflow phenomena. Freyman *et al*[29] reported that intracoronary MSC infusion impaired coronary flow distal to the infusion site in half of their treated pigs. Similar to this report, the intracoronary administration showed elevated cardiac enzymes and micro infarctions in dogs with normal coronary arteries.[30] Hoshino *et al*[18] compared three methods for the injection of gelatin hydrogel microspheres, namely, antegrade injection, retrograde injection, and direct injection. The greatest number of microspheres was retained in the target area after the antegrade injection, but this method induced microinfarctions and failed to show any angiogenic effect. An increased coronary flow reserve was observed in the animals receiving retrograde injection and direct injection therapy, thus confirming the superior efficacy of these methods compared with antegrade injection. Importantly, retrograde injection was much less invasive than direct intramyocardial injection.

Coronary vein infusion of MSCs is a promising therapeutic strategy for the treatment and prevention of heart failure. Yet, the cell implantation failed to reduce cardiac fibrosis or achieve reverse remodeling in this study. Further studies in large animals to explore the methods to enhance or modify MSC function, such as gene transfer[11] and pharmacological preconditioning,[31] will be necessary.

Taken together, our results show that MSC implantation via the coronary vein is feasible and prevents cardiac contractile dysfunction in ischemic cardiomyopathy of pigs. The mechanism behind this benefit appears to be partly attributable to increased local expression of angiogenic factors such as VEGF and enhanced neovascularization in response to the cell implantation.

ACKNOWLEDGEMENTS

We thank Ms Matsuzaki for her technical assistance. This work was supported in part by a Grant-in-Aid for Scientific Research from the Japan Society for the Promotion of Science (to Y Iso).

DISCLOSURE/CONFLICT OF INTEREST

The authors declare no conflicts of interest.

1. Tateishi-Yuyama E, Matsubara H, Murohara T, *et al.* Therapeutic angiogenesis for patients with limb ischaemia by autologous transplantation of bone-marrow cells: a pilot study and a randomised controlled trial. Lancet 2002;360:427–435.
2. Schächinger V, Erbs S, Elsässer A, *et al.* Intracoronary bone marrow-derived progenitor cells in acute myocardial infarction. N Engl J Med 2006;355:1210–1221.
3. Wollert KC, Meyer GP, Lotz J, *et al.* Intracoronary autologous bone-marrow cell transfer after myocardial infarction: the BOOST randomised controlled clinical trial. Lancet 2004;364:141–148.
4. Janssens S, Dubois Ch, Bogaert J, *et al.* Autologous bone marrow-derived stem-cell transfer in patients with ST-segment elevation myocardial infarction: double-blind, randomized controlled trial. Lancet 2006;367:113–121.
5. Lunde K, Solheim S, Aakhus S, *et al.* Intracoronary injection of mononuclear bone marrow cells in acute myocardial infarction. N Engl J Med 2006;355:1199–1209.
6. Iso Y, Soda T, Sato T, *et al.* Impact of implanted bone marrow progenitor cell composition on limb salvage after cell implantation in patients with critical limb ischemia. Atherosclerosis 2010;209: 167–172.
7. Iso Y, Spees JL, Serrano C, *et al.* Multipotent human stromal cells improve cardiac function after myocardial infarction in mice without long-term engraftment. Biochem Biophys Res Commun 2007;354: 700–706.
8. Amado LC, Saliaris AP, Schuleri KH, *et al.* Cardiac repair with intramyocardial injection of allogeneic mesenchymal stem cells after myocardial infarction. Proc Natl Acad Sci USA 2005;102:11474–11479.
9. Lim SY, Kim YS, Ahn Y, *et al.* The effects of mesenchymal stem cells transduced with Akt in a porcine myocardial infarction model. Cardiovasc Res 2006;70:530–542.
10. Nagaya N, Kangawa K, Itoh T, *et al.* Transplantation of mesenchymal stem cells improves cardiac function in a rat model of dilated cardiomyopathy. Circulation 2005;112:1128–1135.
11. Gnecchi M, He H, Liang OD, *et al.* Paracrine action accounts for marked protection of ischemic heart by Akt-modified mesenchymal stem cells. Nat Med 2005;11:367–368.
12. Wolf D, Reinhard A, Seckinger A, *et al.* Dose-dependent effects of intravenous allogeneic mesenchymal stem cells in the infarcted porcine heart. Stem Cells Dev 2009;18:321–329.
13. Krause U, Harter C, Seckinger A, *et al.* Intravenous delivery of autologous mesenchymal stem cells limits infarct size and improves left ventricular function in the infarcted porcine heart. Stem Cells Dev 2007;16:31–37.
14. Makkar RR, Price MJ, Lill M, *et al.* Intramyocardial injection of allogenic bone marrow-derived mesenchymal stem cells without immunosuppression preserves cardiac function in a porcine model of myocardial infarction. J Cardiovasc Pharmacol Ther 2005;10: 225–233.
15. Yokoyama S, Fukuda N, Li Y, *et al.* A strategy of retrograde injection of bone marrow mononuclear cells into the myocardium for the treatment of ischemic heart disease. J Mol Cell Cardiol 2006;40:24–34.
16. Baklanov DV, Moodie KM, McCarthy FE, *et al.* Comparison of transendocardial and retrograde coronary venous intramyocardial catheter delivery systems in healthy and infarcted pigs. Catheter Cardiovasc Interv 2006;68:416–423.
17. Thompson CA, Nasseri BA, Makower J, *et al.* Percutaneous transvenous cellular cardiomyoplasty. A novel nonsurgical approach for myocardial cell transplantation. J Am Coll Cardiol 2003;41:1964–1971.
18. Hoshino K, Kimura T, De Grand AM, *et al.* Three catheter-based strategies for cardiac delivery of therapeutic gelatinmicrospheres. Gene Ther 2006;13:1320–1327.
19. Sato T, Suzuki H, Kusuyama T, *et al.* G-CSF after myocardial infarction accelerates angiogenesis and reduces fibrosis in swine. Int J Cardiol 2008;127:166–173.
20. Jimi T, Wakayama Y, Inoue M, *et al.* Aquaporin 1: examination of its expression and localization in normal human skeletal muscle tissue. Cells Tissues Organs 2006;184:181–187.